

Unsteady Aerodynamic Modeling of Aircraft Control Surfaces by Indicial Response Methods

Mehdi Ghoreyshi* and Russell M. Cummings†

High Performance Computing Research Center, U.S. Air Force Academy, Colorado 80840

DOI: 10.2514/1.J052946

This study is part of a larger effort to create reduced-order models for aerodynamic forces and moments acting on a maneuvering aircraft with moving control surfaces. The aircraft used in this study was inspired by the T-38 jet trainer and includes elevators, rudder, ailerons, and trailing-edge flaps on the wing for landing and takeoff. A hybrid unstructured overset mesh was generated to move these control surfaces and simulate the unsteady flowfields around the aircraft. The static results are first compared to experimental data available at different flap deflection angles, with good agreement obtained at low to moderate angles of attack and deflection angles. Unsteady airloads predictions were then made using the indicial response methods and response functions due to step changes in control surface deflection angles. A time-dependent surrogate model was also used to approximate the response function variation with changes in the angle of attack. The model outputs were then compared with time-accurate simulations of arbitrary control surface motions within the range of data used for model generation. Very good agreement was found between models and computational-fluid-dynamics data for low and high motion rates at low to moderate deflection angles. The results demonstrated that unsteady effects significantly change the amplitude and phase lags of predicted airloads compared with static (or steady-state) predictions.

Nomenclature

a	=	acoustic speed, m/s
b	=	wingspan, m
C_D	=	$D/q_\infty S$, drag coefficient
C_N	=	$N/q_\infty S$, normal force coefficient
C_l	=	$\bar{L}/q_\infty S b$, roll moment coefficient
C_m	=	$\bar{M}/q_\infty S c$, pitch moment coefficient
C_n	=	$\bar{N}/q_\infty S b$, yaw moment coefficient
C_Y	=	$Y/q_\infty S$, side-force coefficient
c	=	mean aerodynamic chord, m
D	=	drag force, N (also input matrix in surrogate model)
k	=	$\omega c/2V$, reduced frequency
$\bar{L}, \bar{M}, \bar{N}$	=	roll, pitch, and yaw moments, N · m
M	=	V/a , Mach number
N	=	normal force, N
q_∞	=	$\rho V^2/2$, freestream dynamic pressure, Pa
Re	=	$\rho V c/\mu$, Reynolds number
S	=	reference area, m ²
s	=	$2Vt/c$, normalized time
t	=	time, s
V	=	freestream velocity, m/s
x, y, z	=	aircraft position coordinates
Y	=	side force, N
Z	=	output matrix of surrogate model
α	=	angle of attack, rad
δ	=	control-surface angle, rad
$\dot{\delta}$	=	control-surface time rate, rad/s
δ_a	=	aileron angle, rad
δ_e	=	elevator angle, rad
δ_f	=	flap angle, rad
δ_r	=	rudder angle, rad
μ	=	air viscosity

ρ	=	density, kg/m ³
ω	=	circular frequency, rad/s

I. Introduction

IN A modern fighter aircraft, control surfaces have to be deflected very rapidly to increase the agility of the aircraft. The transient aerodynamic response of aircraft to these abrupt motions is unsteady and behaves very differently from static values. Generally, the unsteady airloads acting on moving control surfaces include circulatory and noncirculatory components [1]. The noncirculatory loads are related to the effects of added mass due to formation of compression and expansion waves around control surface as it undergoes an unsteady motion [2,3]. As the control-surface motion time progresses, these waves will move away, and therefore noncirculatory loads will decay rapidly. The circulatory loads, on the other hand, are long-time loads and represent the effect of vorticity in the flow due to changes in the forcing function (e.g., angle of attack or deflection angle).

Unfortunately, no analytic solution exists to determine the circulatory and noncirculatory loads acting on aircraft control surfaces. Wind-tunnel experiments and flight testing are quite expensive and typically only available late in the design stage. Wind-tunnel models with moving control surfaces are usually complex geometries, and therefore it takes a long time to plan and complete the tests [4]. Unsteady load measurements in wind-tunnel experiments are limited due to dynamic maneuver limitations in the test facilities [4]. An alternative is simulation of control-surface deflections using computational fluid dynamics (CFD). Recent work [5,6] has demonstrated the CFD approach to simulate a maneuvering aircraft with moving surfaces using time-accurate Reynolds-averaged Navier–Stokes (RANS) equations. These simulations (often referred to as full-order models) are able to compute circulatory and noncirculatory loads acting on aircraft with high accuracy. However, they are computationally expensive for flight-dynamic applications, which require a large number of computations for different values of motion frequency and amplitude for each aircraft configuration. It is therefore desirable to use a relatively simple but accurate approximation for the unsteady aerodynamics by using a reduced-order model (ROM) that allows describing the unsteady flow in the form of a small number of spatial/temporal modes (typically less than 100) compared with the very large number of grid points in the full-order model (on the order of 5 to 50 million or more) [7,8]. The ROMs

Presented as Paper 2013-2535 at the 31st AIAA Applied Aerodynamics Conference, San Diego, CA, 24–27 June 2013; received 17 July 2013; revision received 7 April 2014; accepted for publication 7 April 2014; published online 27 June 2014. This material is declared a work of the U.S. Government and is not subject to copyright protection in the United States. Copies of this paper may be made for personal or internal use, on condition that the copier pay the \$10.00 per-copy fee to the Copyright Clearance Center, Inc., 222 Rosewood Drive, Danvers, MA 01923; include the code 1533-385X/14 and \$10.00 in correspondence with the CCC.

*Senior Aerospace Engineer. Senior Member AIAA.

†Professor of Aeronautics. Associate Fellow AIAA.

used in this paper are based on linear and nonlinear indicial response methods.

The aerodynamic response to a unit step change in the forcing function is the so-called indicial response. Although the indicial response is relatively simple in concept, it is nonetheless useful for predicting unsteady aerodynamics because the response calculation consists of both circulatory and noncirculatory components. The linear response to any arbitrary forcing function can be approximated through the superposition of indicial responses using Duhamel's integral [9]. Wagner [10] was the first to solve the indicial response of a thin airfoil due to a step change in the angle of attack in incompressible flow, the so-called Wagner function. This function is a single, one-parameter function and is sufficient to model the plunging motion of a thin airfoil in linear two-dimensional flow. For a pitching motion, Tobak [11] formulated an indicial response model by adding Duhamel's integrals with respect to angle of attack and pitch rate. Ghoreyshi and Cummings [12] extended the indicial response method of Tobak to predict all aerodynamic forces and moments acting on an aircraft due to six-degree-of-freedom aircraft maneuvers. However, there were no control surfaces modeled during these maneuvers, and indicial functions were calculated only for aircraft states (e.g., angle of attack, side-slip angle, and angular rates). In fact, very few studies have reported results on aerodynamic loads modeling of control surfaces based on indicial theory. This includes the work of Hariharan and Leishman [13], who used the indicial concept for subsonic aerodynamic loads modeling of a flapped airfoil. They used piston theory and linearized subsonic theory to derive indicial functions due to a step change in flap angle and flap rate. However, these functions are valid only for a two-dimensional airfoil in the subsonic speed range. In a recent paper by Nakai et al. [14], a wing aerodynamic response to a step change in the aileron deflection was calculated using CFD. The step functions were then used to predict the unsteady aerodynamics due to small-amplitude aileron motions. The current paper is an attempt to extend these results for aircraft control surfaces. Linear and nonlinear models are developed for elevator, aileron, and flap surfaces of the test case aircraft and tested for arbitrary ramp and pitch motions of control surfaces. A time-dependent surrogate model is also used for aerodynamic modeling in the angle-of-attack/flap-angle space.

II. Methodology

A. Computational-Fluid-Dynamics Solver

The flow solver used for this study is the Cobalt code [15] that solves the unsteady, three-dimensional, and compressible Navier–Stokes equations in an inertial reference frame. In Cobalt, the Navier–Stokes equations are discretized on arbitrary grid topologies using a cell-centered finite-volume method. Second-order accuracy in space is achieved using the exact Riemann solver of Gottlieb and Groth [16] and least-squares gradient calculations using QR factorization. To accelerate the solution of discretized system, a point-implicit method using analytic first-order inviscid and viscous Jacobians is applied. A Newtonian subiteration method is used to improve time accuracy of the point-implicit method. Tomaro et al. [17] converted the code from explicit to implicit, enabling Courant–Friedrichs–Lewy numbers as high as 10^6 . Some available turbulence models are the Spalart–Allmaras model [18], Wilcox's $k-\omega$ model [19], and Mentor's SST model [20].

B. Overset Grid Approach

The simulation of control-surface motions depends on the ability of the CFD solver to model surface deflections. The methods of transpiration, grid deformation, and overset grids have been used for CFD modeling of control surfaces. In the transpiration method, the normal to the deflected surface is used to change the velocity boundary conditions such that the flow solver experiences some sort of deflection in the mesh, although the actual mesh is not deflected [21]. Using this method, the aircraft maneuvers and aeroelastic simulations can be run virtually on the clean configuration grid, and hence the transpiration method drastically reduces the computational cost. However, the surface application of this method is limited to

small deflections of control surfaces [22,23]. Various grid-deformation methods have also been used to deform the volume mesh subject to the surface movement or structural loads [6,24–27]. The most common grid-deformation techniques are transfinite interpolation [26], radial basis functions [25], and the spring analogy [28–31]. However, the deflection of control surfaces using these techniques is limited because the methods could produce distorted grids and often nonrealistic surface grid deformations for large deflection angles.

The overset grid approach has been widely used to deflect control surfaces in CFD as well. In an overset grid, a grid that covers the entire computational domain is named the background grid, and all other grids attached to the control surfaces are called the minor grids [32]. Each minor grid might have interpolation boundary surfaces (IBSs) or fringe boundary surfaces (FBSs) that transfer information between grids. The overset grid module then performs automatic hole cutting by interpolating IBS/FBS in each grid [32]. The overset grid technique could be applied to structured and unstructured grids; however, the number of overlapping grids required for an unstructured grid could be significantly smaller compared with that required for structured grids [33]. The gap regions between aircraft and control surfaces can become an issue with an overset grid approach because the large gaps could exhibit strong flow unsteadiness and affect the predictions [34].

Cobalt uses an overset grid method that allows the independent translation and rotation of each grid around a fixed or moving hinge line. In this method, overlapping grids are generated individually, without the need to force grid points aligned with neighboring components [35]. In Cobalt, the overlapping grids are treated as a single mesh using a grid-assembly process. This includes a hole-cutting procedure in overlapping regions and interpolation between overlapping grids. The translation and rotation of overset grids around the hinge line are input to the code using a grid control file (GCF). The hinge line is defined by a reference point and a vector combination. The rotations are based on the right-hand rule and consist of angles in an order of pitch, yaw, and roll angle. These angles are estimated from the deflection angle of a control surface and the relative angles between the hinge line and grid coordinate axes.

C. Indicial Response Modeling

Indicial response modeling has recently been used for unsteady aerodynamic modeling of maneuvering aircraft [12,36–38]. In all these studies, the indicial functions were calculated only for aircraft states (e.g., angle of attack, side-slip angle, and angular rates), and simulations were performed on the clean configuration grid. This study extends previous work by developing models based on indicial response methods for predicting unsteady aerodynamics of control surfaces. These aerodynamic models are important for a modern fighter aircraft because of the high rates of control-surface deflections. Typical conceptual design aerodynamic predictions have large amounts of uncertainty at these conditions that can lead to unpleasant surprises during prototype flight testing, sometimes requiring the whole aircraft design cycle to be repeated. In addition, these models play an important role in the design of control systems.

The aircraft considered in this study has conventional control surfaces of aileron, elevator, rudder, and a flap surface at the trailing edge of the wing for landing and takeoff. The deflection angles of these surfaces are denoted by δ_a , δ_e , δ_r , and δ_f , representing aileron, elevator, rudder, and flap, respectively. It is assumed that these surfaces move at a fixed approach landing airspeed. The aircraft angular rates and side-slip angle are assumed zero as well. To create a linear ROM, the aerodynamic responses (e.g., normal force, drag, and pitch moment for longitudinal controls) are calculated for a unit step change in the control-surface deflection at a given angle of attack and Mach number. Note that the responses due to a step change in flap motion rate ($\dot{\delta}$) are not considered in this study because the aerodynamic responses to a flap rate are much smaller than responses to a flap angle as shown by Hariharan and Leishman [13]. Also, the flap rate response simulation in CFD includes the effects of both flap angle and rate, and additional work is needed to separate these effects.

For a unit step input, the surface deflection is initially zero and is suddenly deflected 1 deg and held constant at this angle during the remainder of the simulation. The responses to this input function are called the indicial functions and are denoted by $C_{j\delta}$ such that $j = [N, D, m]$ for longitudinal controls and $j = [Y, l, n]$ for lateral controls. These indices represent normal force, drag, pitch moment, side force, roll moment, and yaw moment, respectively. The linear aerodynamic responses to any arbitrary surface deflection can be approximated through the superposition of indicial responses using Duhamel's integral [39]:

$$C_j(t) = C_{j0} + \frac{d}{dt} \left[\int_0^t \delta(\tau) C_{j\delta}(t - \tau) d\tau \right] \quad (1)$$

where C_{j0} are estimated aerodynamic coefficients by setting $\delta(t) = 0$. The indicial functions of $C_{j\delta}(t)$ are usually unknown and need to be determined by some method. For example, Hariharan and Leishman [13] approximated the normal force and pitch moment indicial functions with respect to the flap angle of a flapped thin airfoil. These functions are shown in Fig. 1 for Mach numbers of 0.3 and 0.5. Figure 1 shows that the normal force response has an initial peak such that the peak value is smaller for Mach 0.5. The responses then fall and asymptotically reach their steady-state values. Pitch moment responses also have a negative peak at $s = 0$. The responses

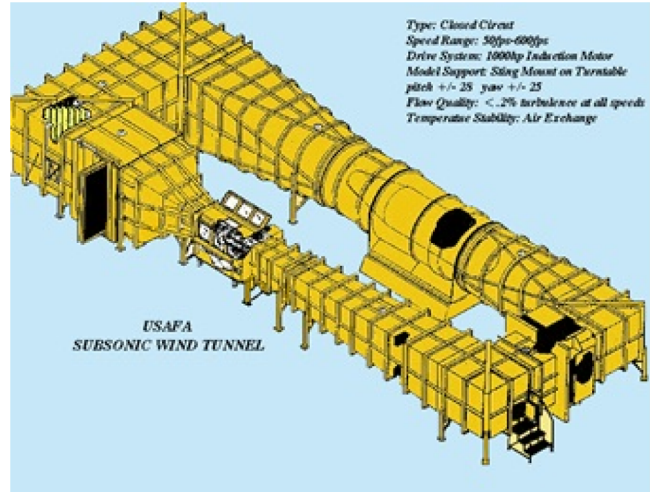


Fig. 3 USAFA subsonic wind-tunnel schematic.

then increase and fall again before reaching steady-state values. Note that these functions are only valid for two-dimensional airfoils.

In this paper, the aircraft indicial functions are calculated using CFD with a grid movement tool. The linear model given in Eq. (1) can

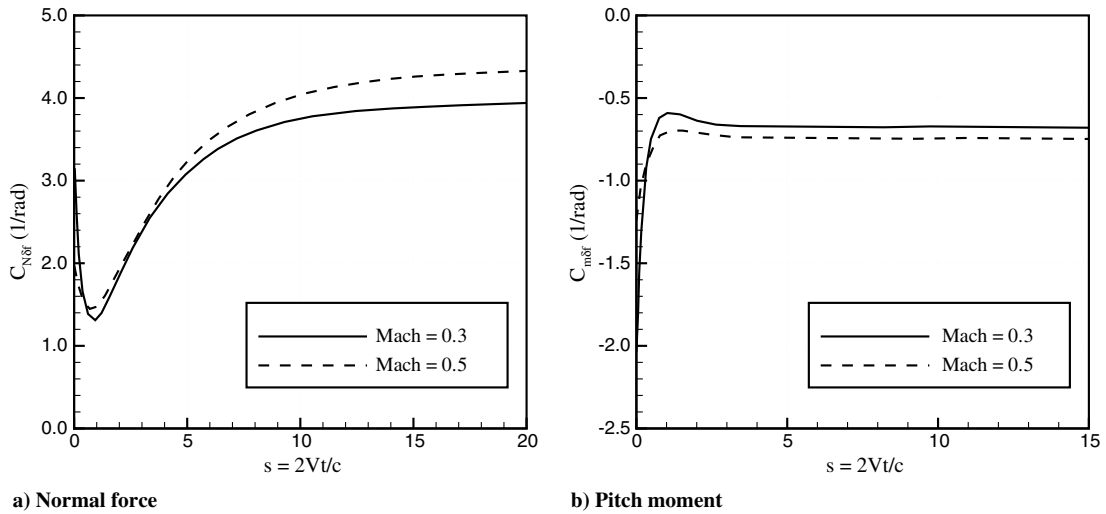


Fig. 1 Indicial normal force and pitch moment of a flapped airfoil due to a unit step change in flap angle (adapted from [13]).

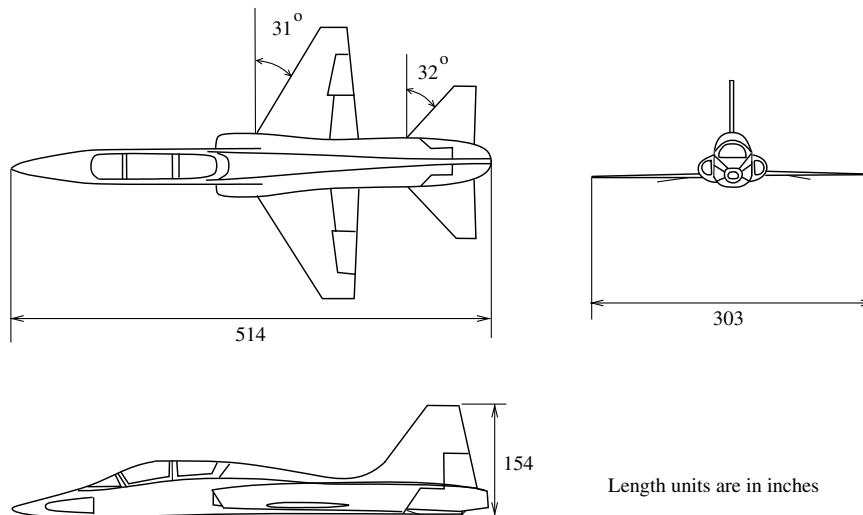


Fig. 2 T-38 Talon aircraft.

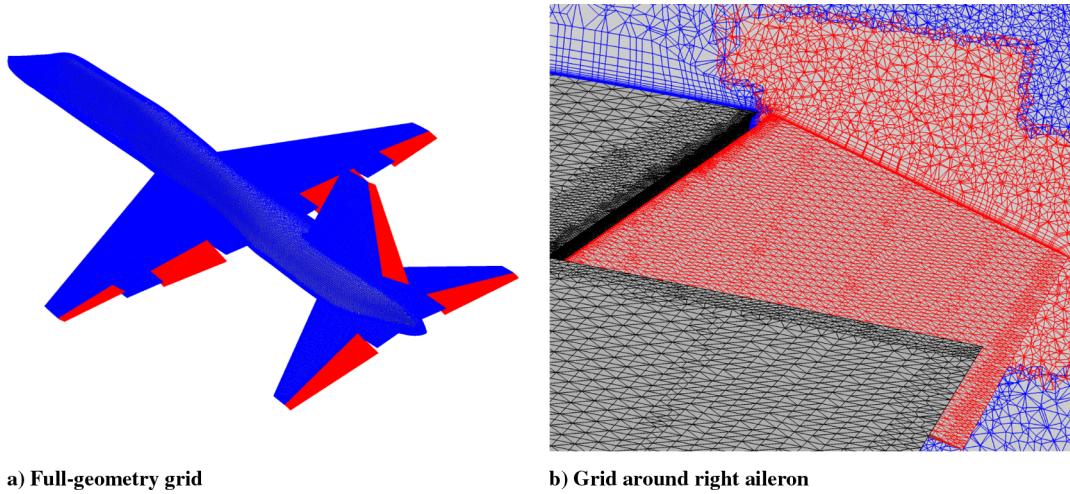
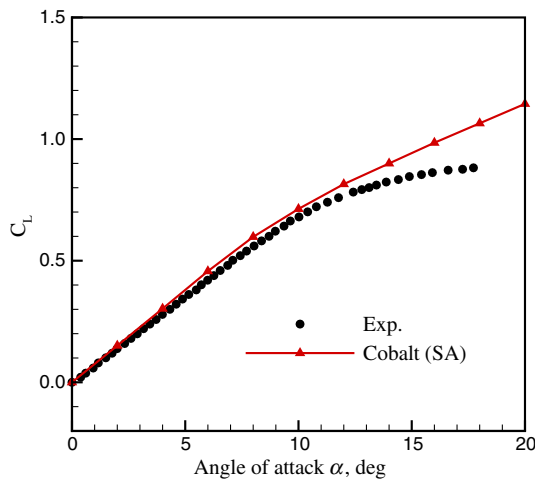


Fig. 4 T-38 overset grid. All control surfaces are deflected ± 15 deg.

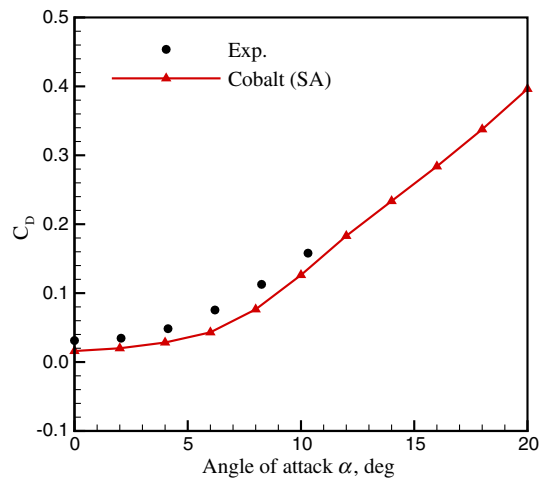
be used for predicting aerodynamics of only small amplitude deflections. A nonlinear model can also be created using indicial functions calculated for different deflection angles. The nonlinear model is written as

$$C_j(t) = C_{j0}(\delta) + \frac{d}{dt} \left[\int_0^t \delta(\tau) C_{j\delta}(t - \tau, \delta) d\tau \right] \quad (2)$$

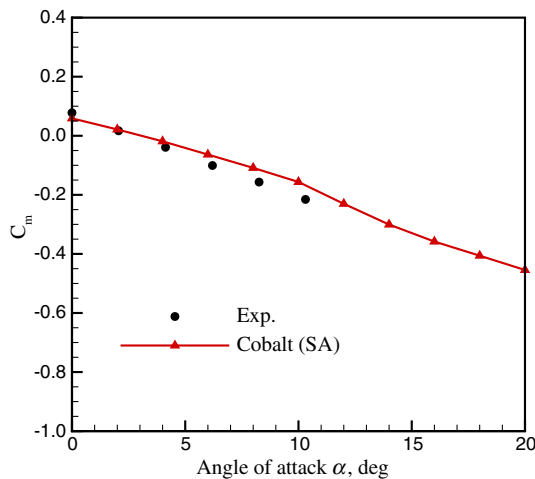
The model in Eq. (2) predicts nonlinear aerodynamic coefficients due to arbitrary control-surface deflections, again at a fixed Mach number and angle of attack similar to those used for estimating indicial functions. The calculation of functions $C_{j\delta}(t - \tau, \delta)$ is as follows: assuming a set of deflection angles of $\delta = [\delta_1, \delta_2, \dots, \delta_n]$, the response functions at each angle of $\delta_i, i = 1, 2, \dots, n$ deg are calculated by holding the deflection angle fixed at $\delta = \delta_i$ deg, and



a) Lift coefficient



b) Drag coefficient



c) Pitch moment coefficient

Fig. 5 Static validation of clean T-38 configuration. Experimental data correspond to a) flight-test data at Mach 0.4, and b-c) wind-tunnel test data at Mach 0.2975.

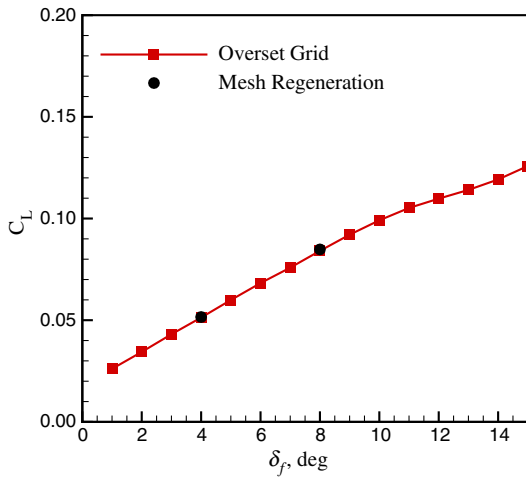


Fig. 6 Static flap surface deflections using overset grid and mesh regeneration: $\alpha = 0$ at Mach 0.4.

then performing a step in the deflection angle to $\delta = \delta_i + \Delta\delta$. The response functions are then computed by taking the differences between the time-varying responses occurring after the step and the steady-state solution at $\delta = \delta_i$ deg and dividing them by the magnitude of the step [40]. These functions are then used to predict the nonlinear effects due to surface deflections in Eq. (2).

Model predictions using Eqs. (1) and (2) are limited by a fixed Mach number and angle of attack used for estimating indicial functions. Approach to landing is a slow flight regime, and therefore

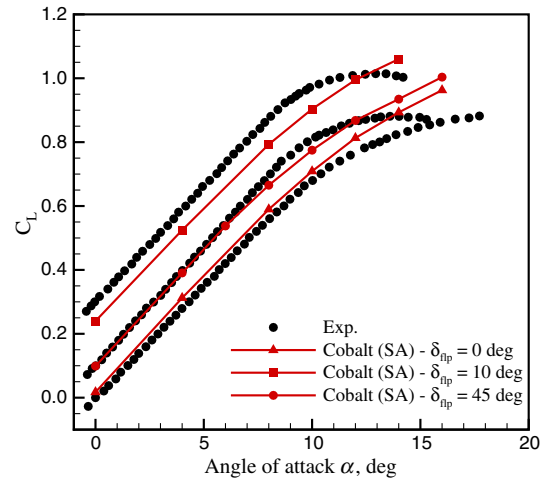
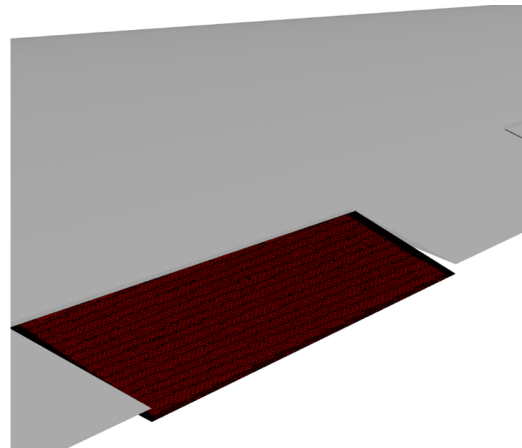


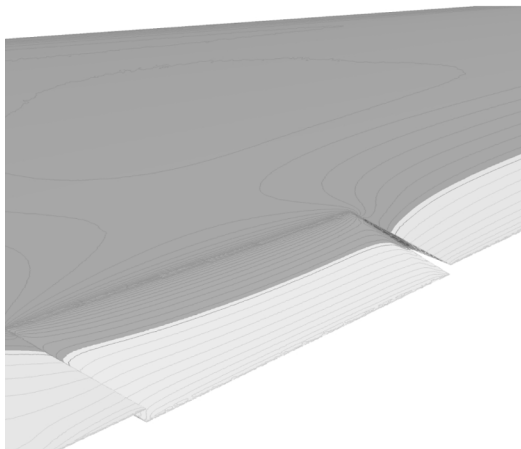
Fig. 8 Static validation of flap surface deflections at Mach 0.4.

Mach number effects on the indicial responses are negligible. However, the indicial functions, and therefore predicted airloads, vary with angle of attack. To extend the indicial response model to include angle of attack effects, the nonlinear indicial functions in Eq. (2) will be calculated for different combinations of δ and α , and therefore Eq. (2) changes to

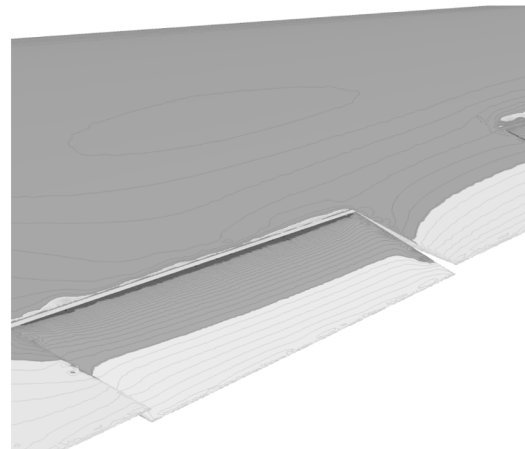
$$C_j(t) = C_{j0}(\delta) + \frac{d}{dt} \left[\int_0^t \delta(\tau) C_{j\delta}(t - \tau, \delta, \alpha) d\tau \right] \quad (3)$$



a) Grids



b) Single mesh surface pressure



c) Overset mesh surface pressure

Fig. 7 Comparison of an overset and a single grid for the flap deflection of 4 deg.

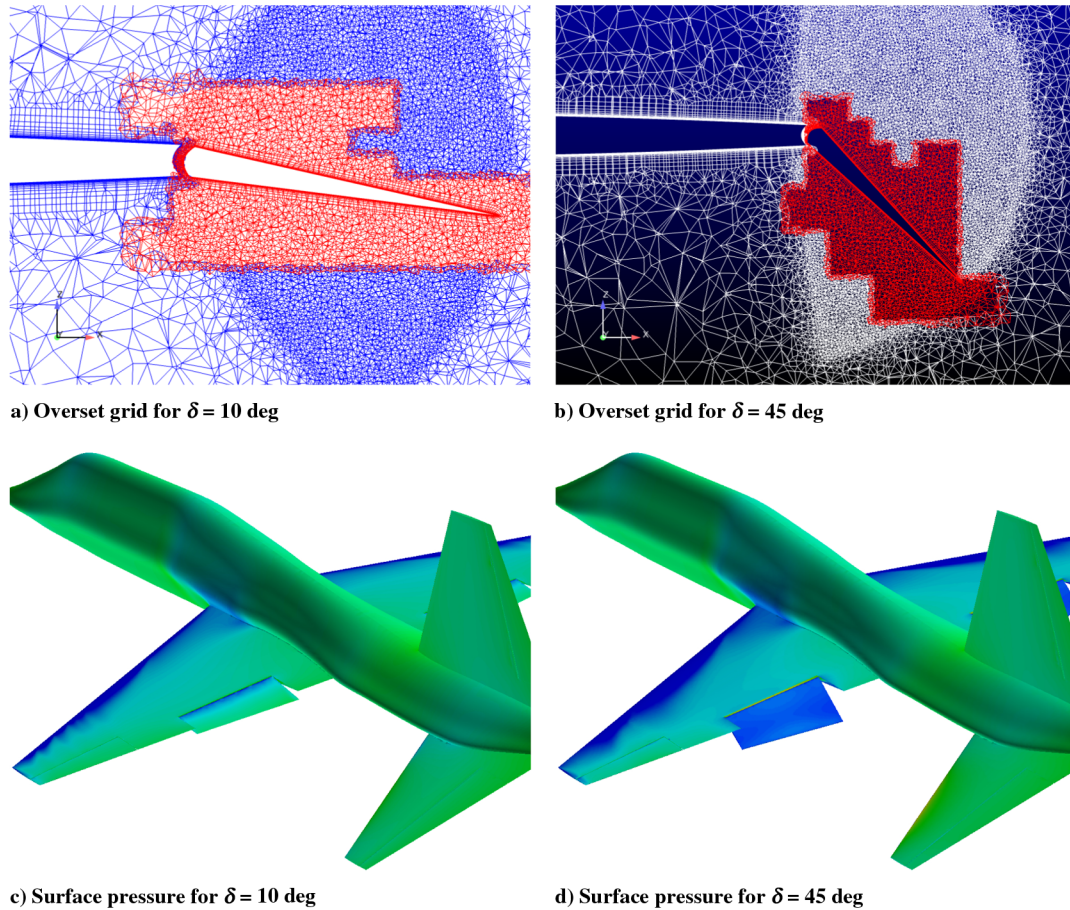


Fig. 9 Overset grid for 10 and 45 deg flap deflections. The pressure solutions correspond to Mach 0.4 and $\alpha = 4$ deg.

However, this model requires a large number of indicial function calculations for each combination of angle of attack and control-surface deflection. To reduce computational cost, a surrogate model is used that estimates indicial functions at a given δ and α from a set of samples (observations). Ghoreyshi and Cummings [12] proposed a surrogate model for aerodynamic modeling of unsteady airloads in the input space of angle of attack and Mach number. This approach is used in this study for aerodynamic modeling in the input space of angle of attack and flap angle.

III. Test Case

The test case is an aircraft inspired by the Northrop T-38 Talon (shown in Fig. 2), which is a two-seat advanced jet trainer powered by two J85-GE-5 turbojet engines [41]. The T-38 aircraft has a ceiling of 50,000 ft and a climb rate of 34,000 ft/min, and it can fly at speeds as high as Mach 1.2, and so it became the world's first supersonic trainer. The vehicle is a variant of the F-5A tactical fighter [42], with a conventional design featuring a swept wing with an area of $S = 170$ ft², a span of $b = 25.25$ ft, an aspect ratio of 3.75, and a taper ratio of 0.2, and it uses the NACA 65A-004 airfoil section. The aircraft model was constructed from a small number of design parameters to describe the T-38 in the Jet Designer code, which is a low-fidelity code developed at the U.S. Air Force Academy (USAFA) for the design of jet fighter aircraft. The aircraft geometry parameters in Jet Designer include lifting surfaces and a fuselage; the fuselage is defined using 20 cross sections. The lifting surfaces are defined using the apex position and placement, leading-edge sweep angle, dihedral angle, span, wing area, and taper ratio. The vertical tail can have a lateral displacement with a tilt angle. A number of aircraft can be defined using this definition; however, the aerodynamic prediction tools available in the code are limited to straight-wing and conventional aircraft configurations.

The surface modeling was performed by SUMO, which produces a surface model and its triangulation. The model can then be passed to an extended CAD system or mesh generator as a standard CAD interface file, and the surface mesh is passed to a tetrahedral volume mesh generator. The SUMO code is a rapid geometry modeling tool for parametrically defined aircraft configurations. The code has a library of geometric primitives based on B-spline curves and surfaces to create a parameterized watertight surface model of the complete jet aircraft. The way SUMO defines a control surface is to input the inboard and outboard span locations as well as chord lengths. The automatic mesh generation tool in SUMO provides an unstructured surface mesh. The mesh control parameters are estimated from the model geometrical features, such as radii of curvature and the presence of sharp edges. From the surface mesh, unstructured volume meshes can be automatically generated using the tetrahedral mesh generator TetGen.[‡]

The static experiments for the T-38 aircraft were conducted in the Subsonic Wind Tunnel facility at USAFA. This closed-loop tunnel as shown in Fig. 3 has an 8-ft-long test section with a test cross section of 3 by 3 ft. The tunnel can achieve speeds in excess of Mach 0.5. The flow conditions in the experiments were $M = 0.2975$, $Re = 6.4 \times 10^5$, and $\beta = 0$. The T-38 wind-tunnel model has a wingspan of 16.5 in., and a mean aerodynamic chord of 5.05 in. Flight-test data at 30,000 ft are also available from Brandt et al. [41] for clean and flapped T-38 configurations. The data correspond to $M = 0.4$ and flap angles of 0, 10, and 45 deg.

Two hybrid-grid RANS meshes were generated from the half- and full-geometry models of the aircraft without control surfaces and engine air inlet. The grids for elevator, rudder, aileron, and flap are generated separately and overset onto the main grids. These grids were generated in two steps. In the first step, the inviscid tetrahedral mesh was generated using the ICEMCFD code. This mesh was then

[‡]Data available at <http://wias-berlin.de/software/tetgen/> [retrieved June 2014].

used as a starting mesh by TRITET [43,44], which builds prism layers using an advancing front technique. TRITET rebuilds the inviscid mesh while respecting the size of the original inviscid mesh from ICEMCFD. In this study, the half-geometry grid was used for flap and elevator aerodynamic modeling, and the full-geometry grid was used for modeling aileron deflections. The assembled grid of the full geometry is shown in Fig. 4a, which has approximately 25.8 million points and 77.7 million cells. Figure 4b also shows the grid around right aileron surface deflected 15 deg. The gaps between the wing and aileron can be seen in this figure. The cross-section plane in Fig. 4b shows how the aileron grid is overset to the background grid.

IV. Results

All simulations in this study were performed using the Spalart–Allmaras turbulence model and were run on either the Cray XE6 computer at the Engineering Research Development Center (computer name is Garnet with 2.7 GHz core speed) or the U.S. Air Force Research Laboratory (Spirit computer with 2.6 GHz core speed).

A. Static Aerodynamic Modeling

The lift, drag, and pitch moment predictions from Cobalt for the T-38 are compared with wind-tunnel and flight-test measurements in Figs. 5a–5c. Wind-tunnel measurements are limited to 10 deg angle of attack, and only lift flight-test data are available. Note that there is no flow through the air intakes for the wind-tunnel model. The figures show that RANS predictions match quite well with the experimental

data at low and moderate angles of attack. However, there are some discrepancies at higher angles, most likely due to geometry differences between the Jet Designer model and the actual T-38 geometry. It should be noted that the purpose of this work is not to investigate the effects of geometry details, grid resolution, numerical parameters, or turbulence modeling requirements for making accurate predictions to match the T-38 aircraft experiments. Therefore, the accuracy of ROM predictions will be assessed by comparison of model outputs with time-accurate CFD simulations, using the same geometry and numerical model settings.

To assess the overset grid approach and to evaluate the effect of gaps between surfaces on predictions, the predictions using overset grid are compared with single meshes regenerated from 4 and 8 deg flap deflections, as shown in Fig. 6. Figure 6 shows that lift coefficients from the single meshes match very well with predictions of flap deflections using the overset grid approach. Figure 7 compares the grid surfaces and the pressure on the wing around the flap with 4 deg of deflection. Figure 7a shows that deflected flap surfaces match with each other, verifying that the calculated GCF angles are correct. Figures 7b and 7c show that the overset grid solution produces similar pressure contours as the single mesh, although there are some differences because of the gaps in the overset grid between the wing, flap, and aileron. However, Fig. 6 shows that the effect of these gaps on the computed normal force are very small at these flight conditions.

Flight-test lift data are also available for a flapped T-38 aircraft at $M = 0.4$ and 30,000 ft altitude with flap settings of 10 and 45 deg. Figure 8 compares the CFD predictions using overset grids with these measurements. Figure 8 shows that the flight-test lift is increased with

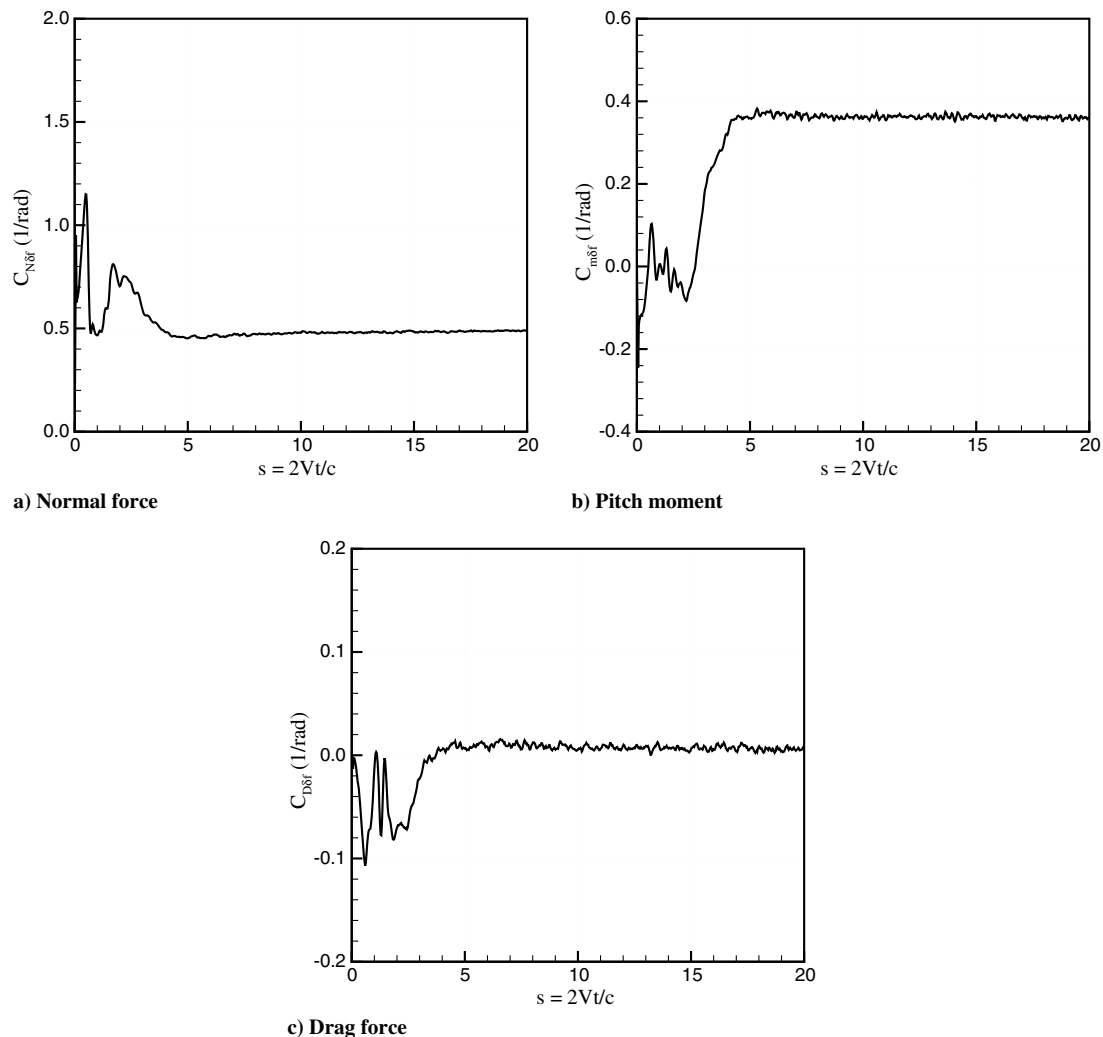
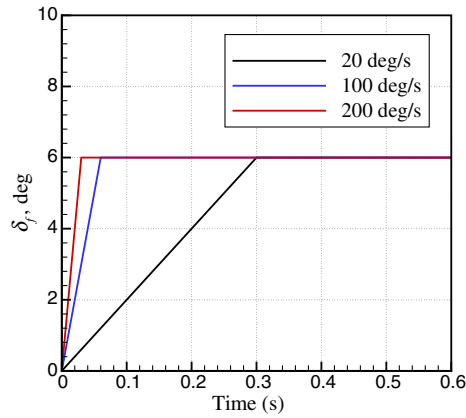
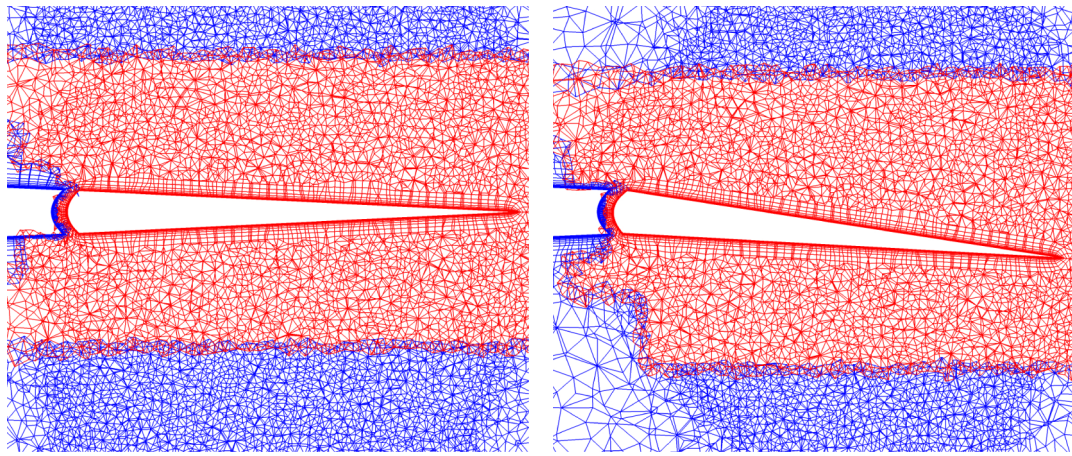


Fig. 10 Indicial responses due to a unit step change in flap angle at 0 deg angle of attack.



a) Ramp flap motions



b) Grid of $\delta_f = 0$ deg

c) Grid of $\delta_f = 6$ deg

Fig. 11 Ramp-flap motions with grids shown at initial and final times.

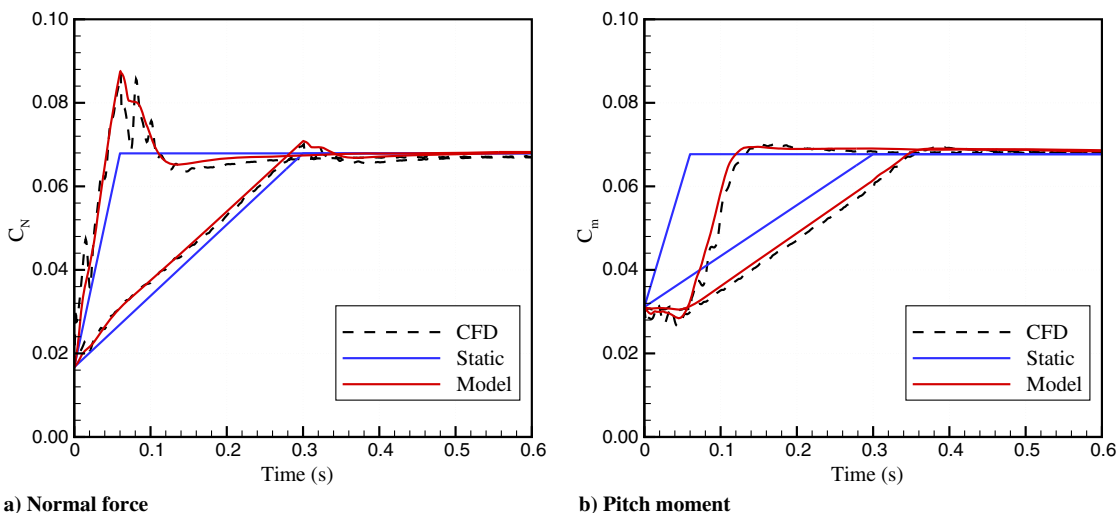
increased flap angle, although the rate of increase is reduced at the larger flap angles. Note that the lift curve slope is nearly unchanged with flap deflection. A good match is found for low to moderate flap angles, but the current approach underestimates measurements at the largest flap angle. The grid assemblies for flap deflections of 10 and 45 deg are shown in Figs. 9a and 9b, respectively. For 4 deg angle of attack, the surface pressure distributions for the aircraft are shown in Figs. 9c and 9d. The figures show that low pressure develops over the upper flap surface behind the hinge line as the flow accelerates over the flap upper surface.

B. Unsteady Aerodynamic Modeling

In all subsequent simulations, the freestream velocity was fixed at a Mach number of 0.1967, corresponding to actual aircraft speeds during approach to landing. The Reynolds number is 1.08×10^7 at standard sea-level conditions. All indicial response functions are calculated at these flight conditions.

1. Aerodynamic Modeling at α Equal to Zero Degrees

The indicial response methods will now be used for aerodynamic modeling of the T-38 aircraft control surfaces. Linear models are first



a) Normal force

b) Pitch moment

Fig. 12 Aerodynamic modeling of flap ramp motions with rates of 20 and 100 deg /s at 0 deg angle of attack.

created from aerodynamic responses to a unit step change in the control-surface deflection. The motion files were generated for these step functions with GCF angles at discrete time instants as input to these files. At each computational time step, Cobalt then interpolates the flap control-surface motion data using cubic splines and moves the control-surface grid, followed by a grid-assembly process. All computations are started from a steady-state solution and clean configuration at 0 deg angles of attack and then advanced in time using second-order accuracy with five Newton subiterations. Time-step size is set to 5×10^{-4} seconds based on a sensitivity study of the grid in [45]. Note that noncirculatory loads occur over a short period of time, and hence a relatively small time step is needed for accurately calculating these loads. On the other hand, choosing too small a time-step size greatly increases the computational cost without adding significant benefit.

The indicial normal force, drag, and pitch moment responses to a unit change in flap deflection are plotted versus normalized time in Fig. 10. Normalized time is defined as $s = 2Vt/c$, where V is the freestream velocity and c is the mean aerodynamic chord. Figure 10 shows that the indicial normal force has an initial jump as the grid starts to rotate, followed by a transient solution. As time progresses, the normal force asymptotically reaches the steady-state value at 1 deg flap angle. The initial peak can be explained based on the energy of acoustic wave systems created by the initial grid perturbation [45]. The pitch moment also has an initial negative peak and a transient solution until it reaches the steady-state value.

Figure 10 shows that the final-time pitch moment response is positive due to the location of the flap relative to the moment reference point. This means a positive flap deflection yields a nose-up pitch moment. Also, Fig. 10 shows that the drag response is small, and therefore drag force changes will not be modeled in this study. It is important to note that the lift and pitch moment indicial functions of the test case aircraft exhibit very different behavior from the flapped airfoil responses shown in Fig. 1. The initial loads are smaller for the test case aircraft; the normal force response of the aircraft reaches the steady-state solution much faster than the airfoil. Steady-state solutions at the final time of motion are different for the aircraft and airfoil as well.

The indicial responses shown in Fig. 10 are substituted into Eq. (1) to predict linear aerodynamic responses of the aircraft to ramp-flap motions. All of these motions start from a clean configuration, and the flap is deflected to 6 deg with rates of 20, 100, and 200 deg/s. The flap is then held constant at 6 deg after the unsteady motion, as shown in Fig. 11a. The assembled grids for the initial and final time are also shown in Figs. 11b and 11c. The motion files in Cobalt are generated using the data values in Fig. 11a. These files define the flap grid rotations around the hinge line at discrete motion time instants. Cobalt then interpolates the motion data using cubic splines and deflects the flap grid for each computational time step. The CFD solver reports time-dependent aerodynamic forces and moments in an inertial axis for each grid; the forces and moments from all grids are added to find the total airloads acting on the aircraft. These

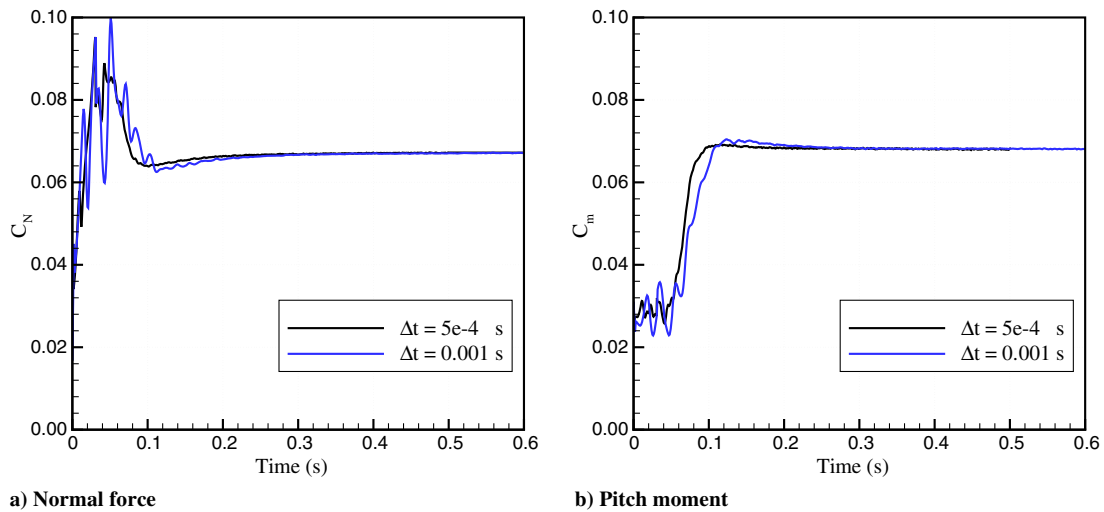


Fig. 13 Time-step size effects of responses of the very fast ramp-flap motion.

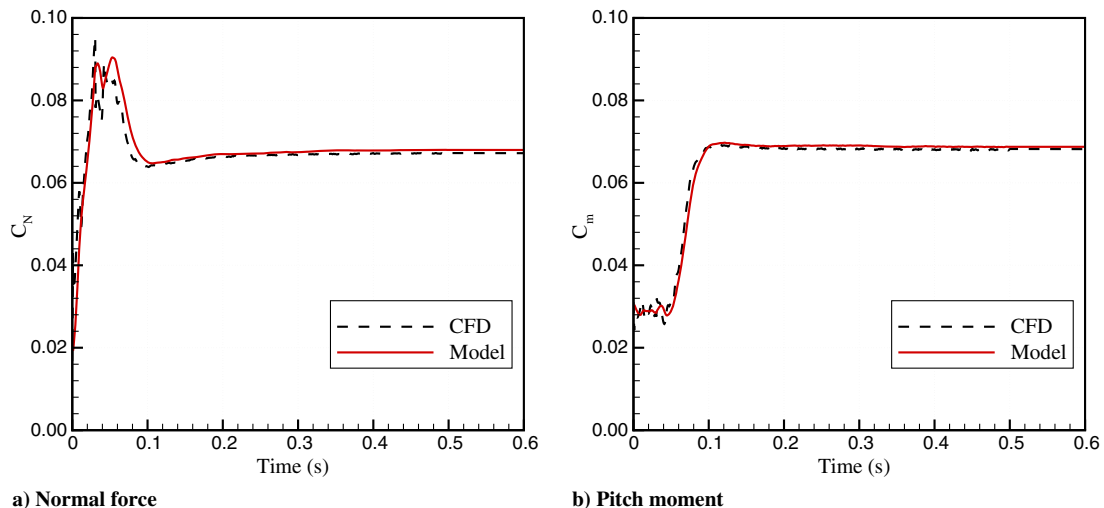


Fig. 14 Aerodynamic modeling of the very fast ramp-flap motion at 0 deg angle of attack.

solutions are labeled “CFD” in the plots. Steady-state solutions are estimated for the input flap angles and are labeled “static” in the plots. Figure 12 compares the model predictions of Eq. (1) with CFD and static solutions of ramp motions with rates of 20 and 100 deg/s. The results show that the indicial response model matches the CFD predictions very well for slow and fast motions. On the other hand, the static predictions fail to predict the transient behavior seen in the CFD. In fact, changes in the static data are synchronized with the flap angle changes, and therefore the static data cannot predict any transient responses. Figure 12 shows that the flap is held constant after ramp motion, but it takes some time before the solution reaches the steady-state value. Also, the normal force during this time is much higher than steady-state values. The transient time and loads increase with the motion rate; the peak normal force of the fast motion is around 30% higher than the steady-state normal force at the final time. The unsteady effects on pitch moment are interesting as well; Fig. 12b shows that the pitch moment response lags in time behind the input. Again, the static data cannot predict this time lag. These results confirm the need to develop unsteady aerodynamic models for aircraft control surfaces.

In the motion with 200 deg/s rate, the flap is deflected from 0 to 6 deg in 0.03 s. The noncirculatory loads are significant for this motion, and the solution is very sensitive to the time-step size. Figure 13 shows the effects of the time step on the CFD solution such that a large time step results in large oscillations in the solution. The small time-step solutions are then compared with the model prediction in Fig. 14. Even for this very fast motion, the model agrees well with the CFD prediction. It should be noted that the flap indicial

responses are time-dependent, and therefore the ROMs using these responses can predict the effects of motion rates as well. The models using Eq. (1) can predict linear aerodynamic response to any arbitrary motion within the range of data used for the model generation. For example, Fig. 15 compares the model predictions with two fast but small amplitude pitch-flap motions. A clockwise hysteresis loop is formed in the plot of normal force against flap angle; the hysteresis loop is introduced in the pitch moment as well, but it is counterclockwise. The results show that the indicial response models accurately predict the CFD data even for the noncirculatory loads that take place at initial time of the motion.

Aerodynamic models are created for the aileron as well. Again the responses to a unit step change in the aileron angle are calculated from CFD. In these calculations, the response solution is started from a clean configuration, and then right and left aileron angles are changed impulsively to 1 and -1 deg, respectively. The time-dependent solutions to this motion are shown in Fig. 16 for side-force, yaw, and roll moments. The normal force and pitch moment response to aileron angle changes are small and are not considered. The results show that the responses have large oscillations initially and then reach the steady-state solutions at 1 deg aileron angle. However, the side-force and yaw moment responses are much smaller than the roll moment response; this confirms that aileron deflection produces more important changes to the roll moment. The roll moment response at the final simulation time is negative; therefore, a positive aileron produces a negative roll moment, as expected. The roll moment indicial function is used to create a ROM and predict responses to two ramp aileron motions with rates of 20

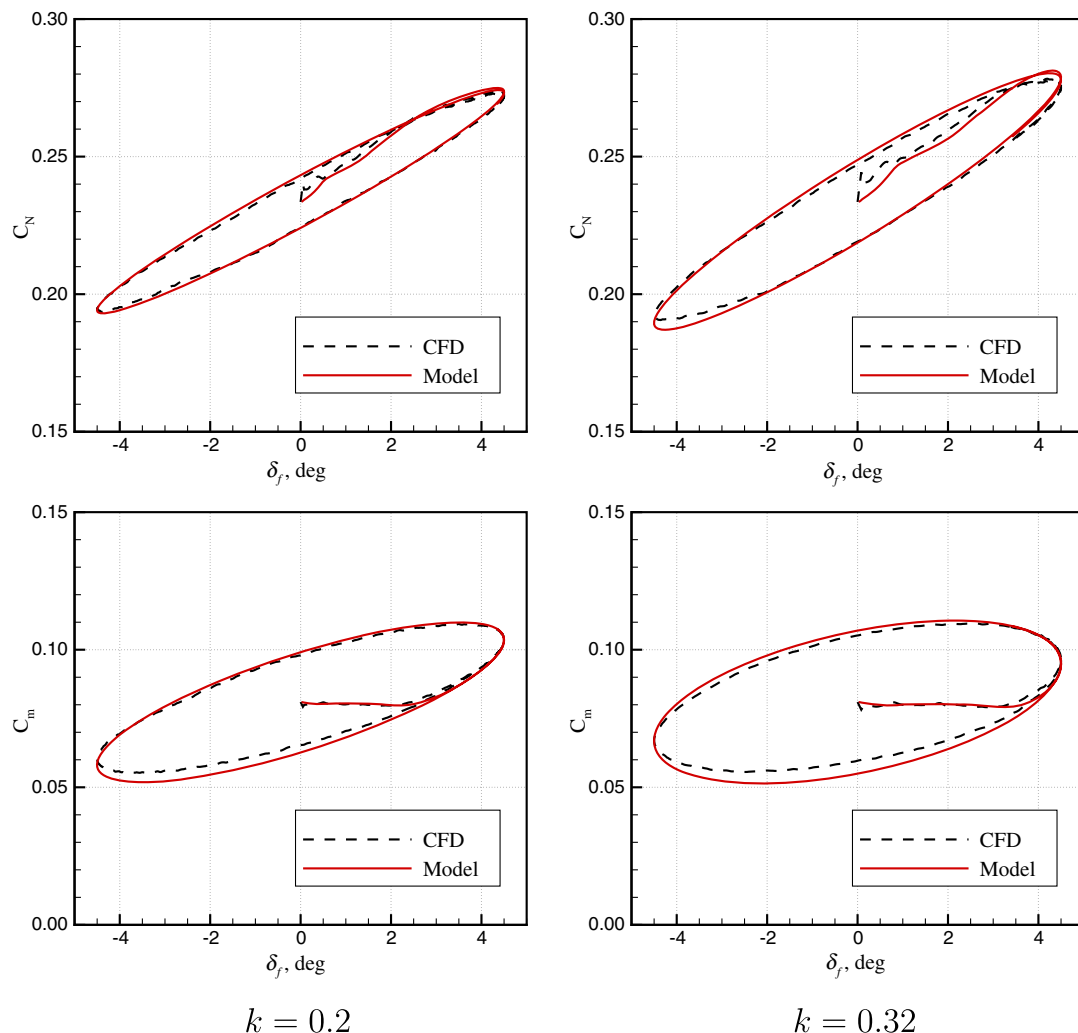


Fig. 15 Aerodynamic modeling of pitch-flap motions at 0 deg angle of attack. Motions are defined as $\delta_f(t) = 4.5 \sin(\omega t)$ with reduced frequencies of $k = 0.2$ and 0.32 , where $k = \omega c/2V$.

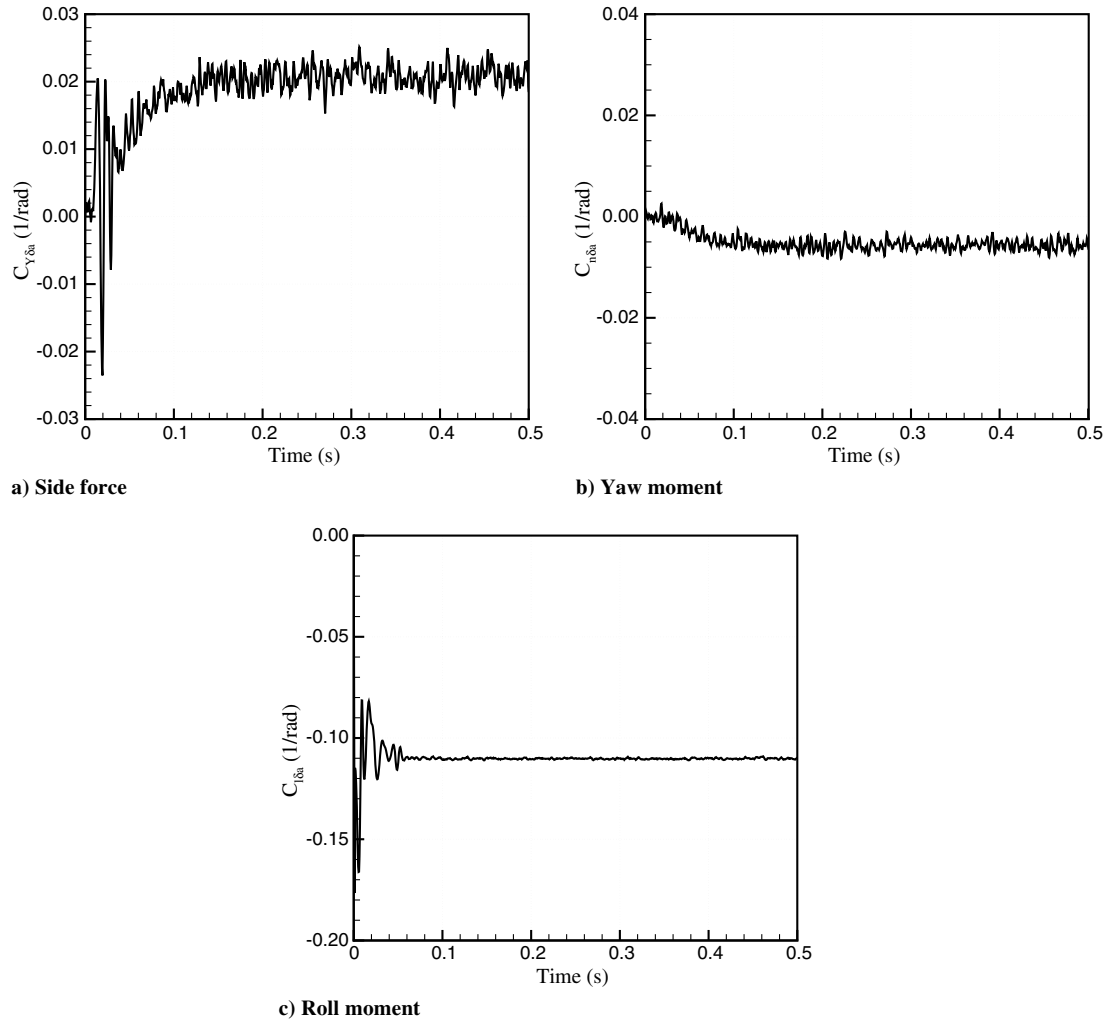


Fig. 16 Indicial responses due to a unit step change in aileron angle at 0 deg angle of attack.

and 100 deg/s. These motions are shown in Fig. 17a, where the aileron is at 0 deg at $t = 0$ and then increases until it reaches 6 deg and is then held constant at this angle. Figure 17b compares the model predictions with roll moment data calculated from CFD. Again, a very good agreement is found in both motions.

Elevator indicial functions are shown in Fig. 18 for normal force and pitch moment. Like the flap responses shown earlier, the solutions predict an initial peak followed by a transient behavior until

they reach the steady-state values at 1 deg elevator angle. The normal force final time value is close to the one found for the flap in Fig. 10a, but the pitch moment values are different for elevator and flap deflections; the pitch moment magnitude is larger for the elevator deflection, and it reaches a negative value because of the location of the elevator relative to the moment reference point. These indicial functions are used to predict the linear aerodynamic response of the T-38 aircraft to two ramp elevator motions. These motions, shown in

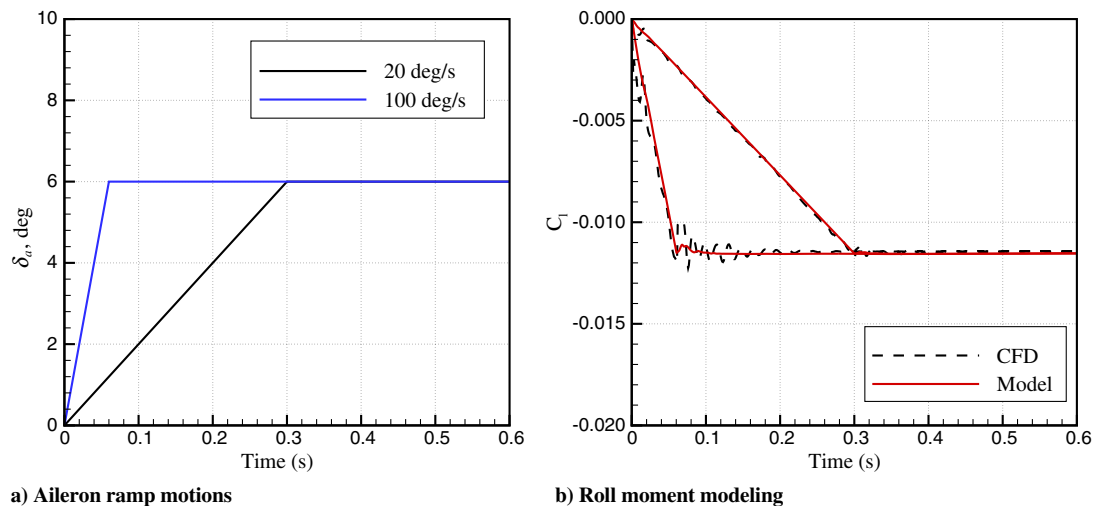


Fig. 17 Roll moment modeling of aileron ramp motions at 0 deg angle of attack.

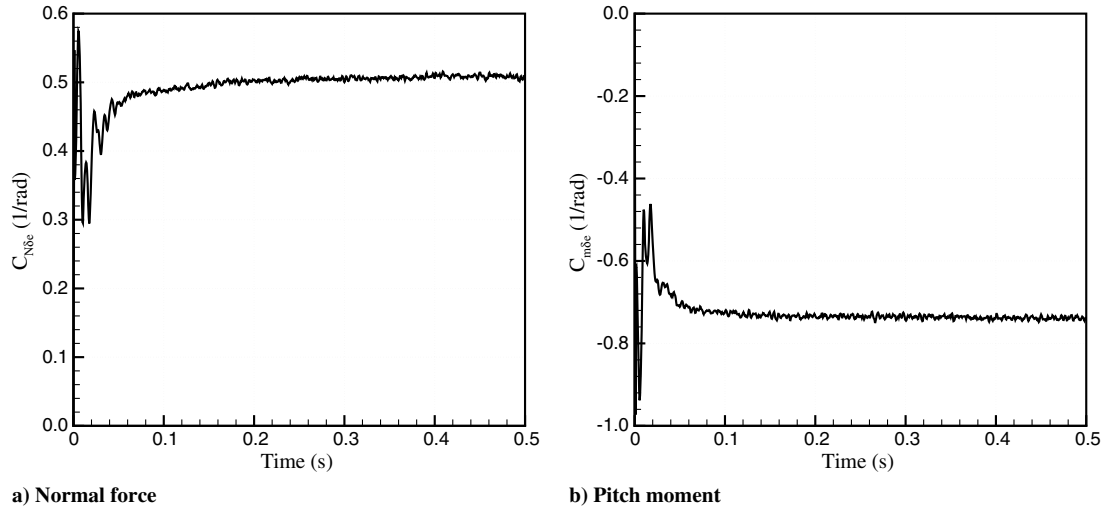
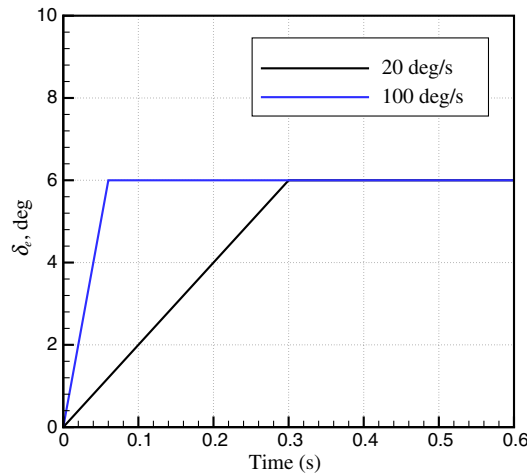


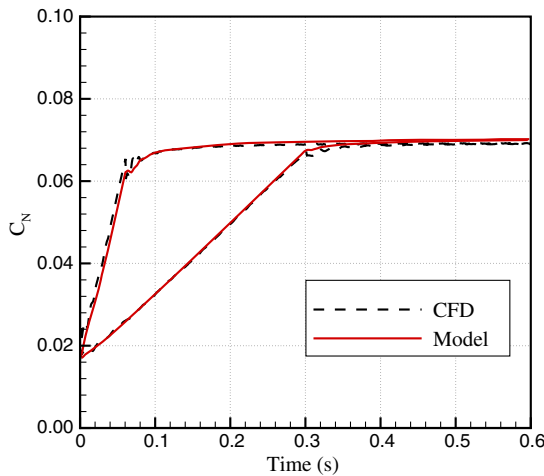
Fig. 18 Indicial responses due to a unit step change in elevator angle at 0 deg angle of attack.

Fig. 19a, are for elevator deflection increasing from 0 to 6 deg with rates of 20 and 100 deg/s. The elevator is then held constant at 6 deg after the ramp motion. The CFD (full-order) prediction and model predictions of these motions are compared in Figs. 19b and 19c for the normal force and pitch moment. These figures show the model output matches with the CFD very well.

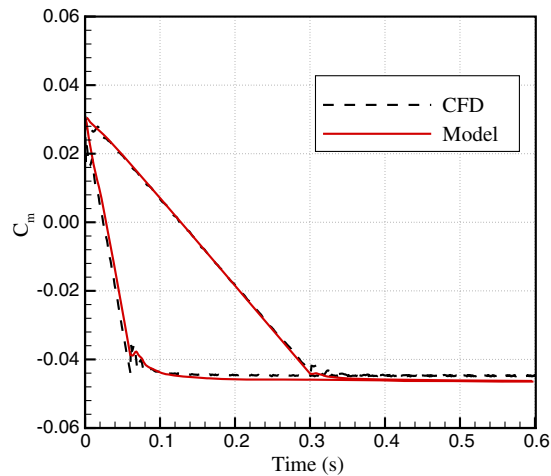
The indicial responses shown in Figs. 10a and 10b are sufficient to model the normal force and pitch moment acting on the test case aircraft due to small-amplitude flap motions. For accurate modeling of large-amplitude motions, the responses to higher flap angles are required. The interval indicial functions are used in this study to calculate the dependency of the reduced-order model on the flap



a) Elevator ramp motions



b) Normal force modeling



c) Pitch moment modeling

Fig. 19 Aerodynamic modeling of elevator ramp motions at 0 deg angle of attack.

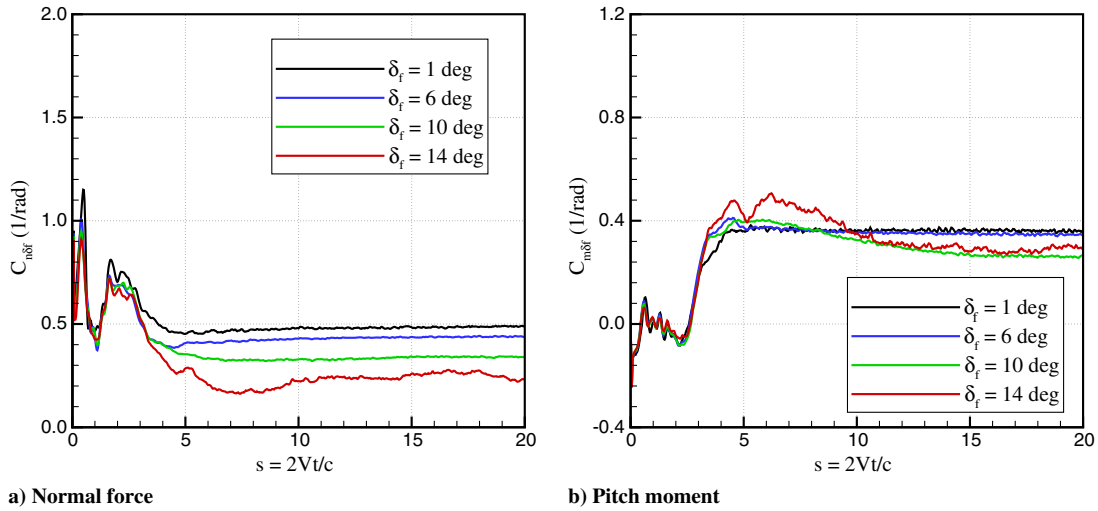
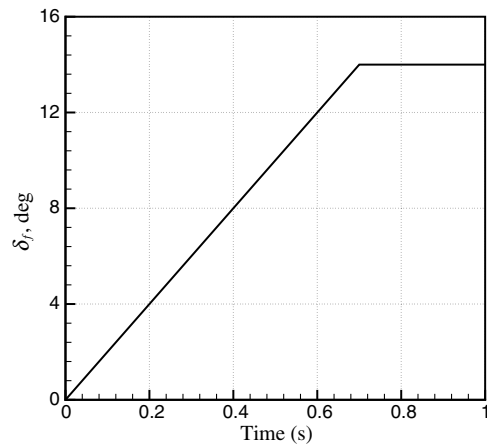


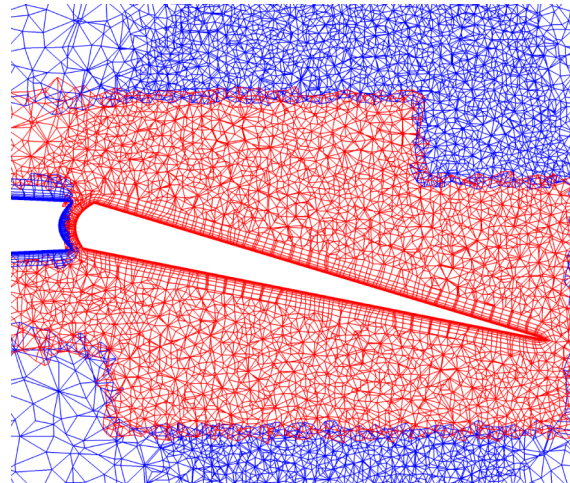
Fig. 20 Nonlinear flap indicial responses at 0 deg angle of attack.

angle. For example, to find the nonlinear response between flap angles of 8 and 10 deg, the solution starts from a steady-state condition with the flap deflected 8 deg and then performs a unit step in the flap angle for all $t > 0$. The response functions are then computed by taking the differences between the time-varying lift and pitch moments occurring after the step and the steady-state solution at $t = 0$ and dividing them by the magnitude of the step, which is 1 deg. For a weakly nonlinear system, the response will be independent of

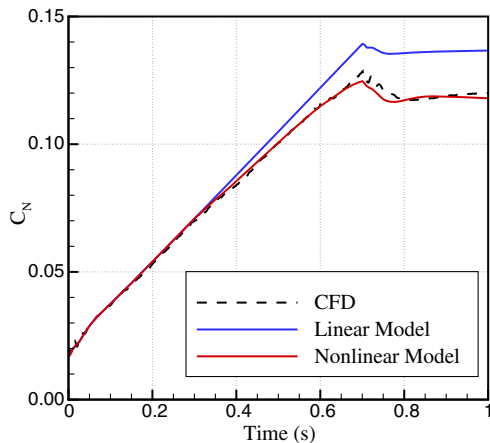
the step magnitude, but for a highly nonlinear system, the interval indicial functions depends on the interval length and the step magnitude. The nonlinear ROM used in this study is valid for weakly nonlinear regimes of flow. Nonlinear response functions are shown in Fig. 20 for different flap angles. Figure 20 shows that the initial time values are nearly independent of flap angle because they are related to the formation of expansion and compression waves around the aircraft as the flap starts to rotate. However, the transient and final



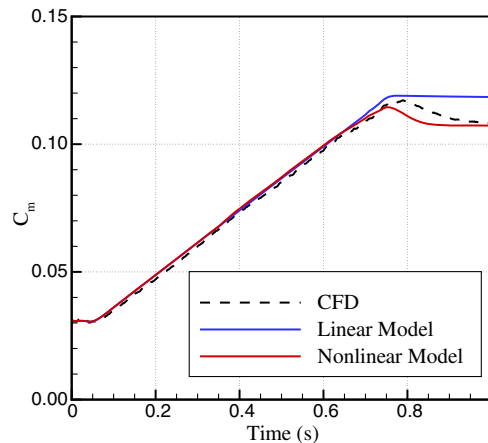
a) Flap ramp motion



b) Grid of $\delta_f = 14$ deg



c) Normal force modeling



d) Pitch moment modeling

Fig. 21 Nonlinear aerodynamic modeling of a flap ramp motion at 0 deg angle of attack.

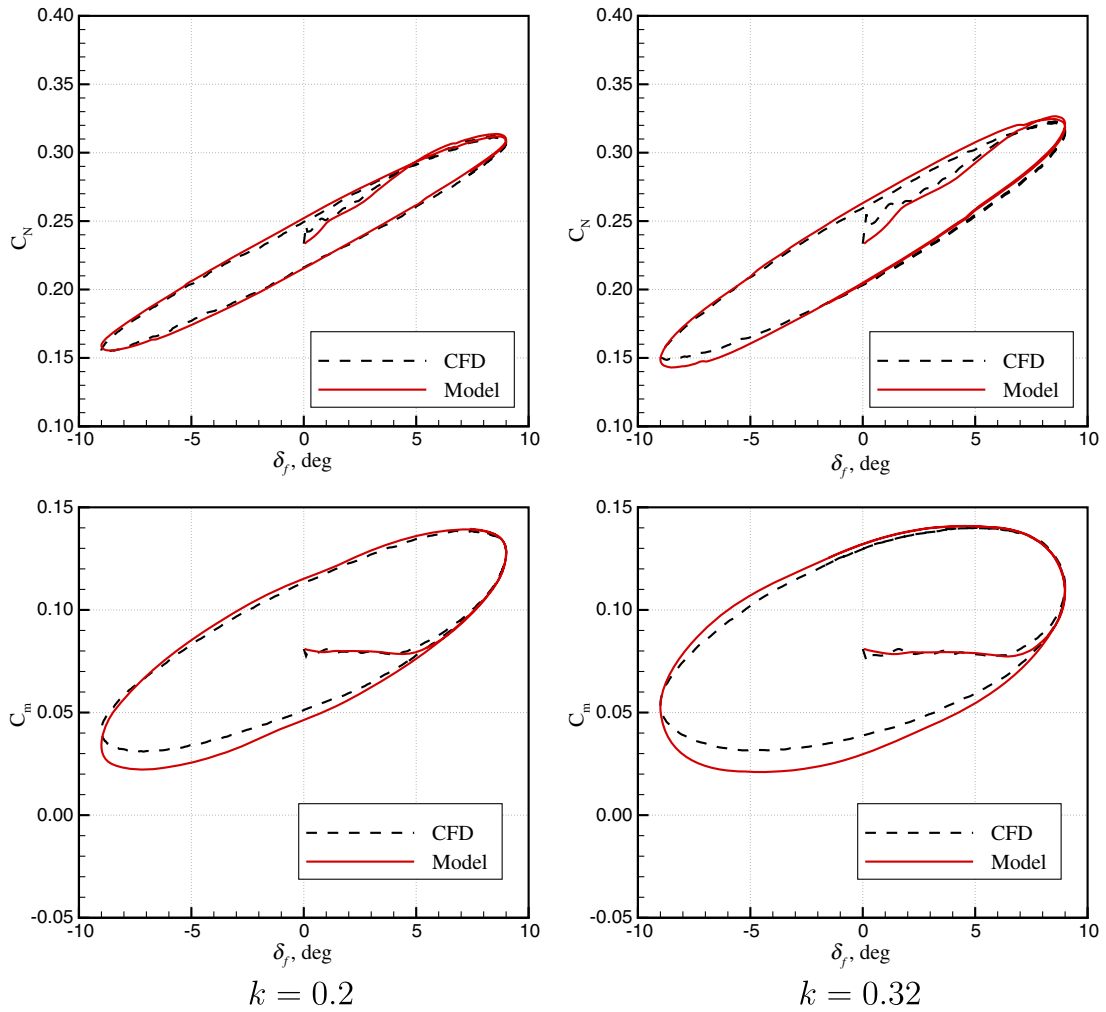


Fig. 22 Nonlinear aerodynamic modeling of pitch-flap motions at 0 deg angle of attack. Motions are defined as $\delta_f(t) = 9.0 \sin(\omega t)$ with reduced frequencies of $k = 0.2$ and 0.32 , where $k = \omega c/2V$.

solutions vary with flap angle such that the final time values of the normal force responses decrease with increasing flap angle. The pitch moment response exhibits a more nonlinear behavior than normal force. The steady-state values decrease with flap angle and then increase. This makes pitch moment modeling of large flap angles a more difficult task than modeling normal force. Nonlinear ROMs are created for the normal force and pitch moment using Eq. (2), and the responses are shown in Fig. 20. The linear and nonlinear model

predictions are then compared with CFD predictions of the two ramp-flap motions in Fig. 21. In these motions, the flap is deflected from 0 to 14 deg with rates of 20 and 100 deg/s and is then held constant at 14 deg for all subsequent time. Figure 21 shows that linear models overestimate the lift and pitch moment at large flap angles because of the linear assumptions made in the model. The nonlinear models have a much better match with CFD, especially for normal force, but they are more expensive than linear models because they require more

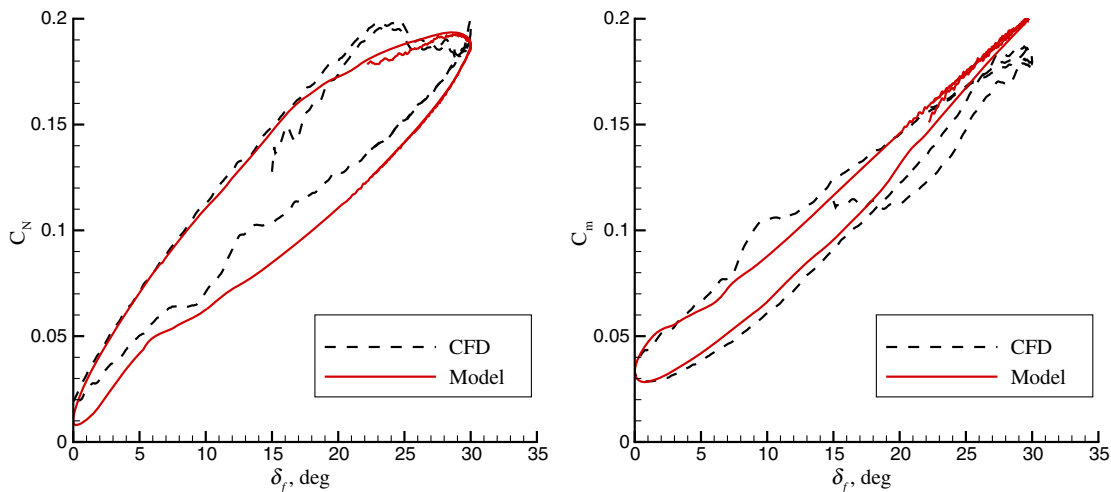


Fig. 23 Nonlinear aerodynamic modeling of a pitch-flap motion defined as $\delta_f(t) = 15.0 + 15.0 \sin(\omega t)$ with reduced frequency of $k = 0.098$ at 0 deg angle of attack.

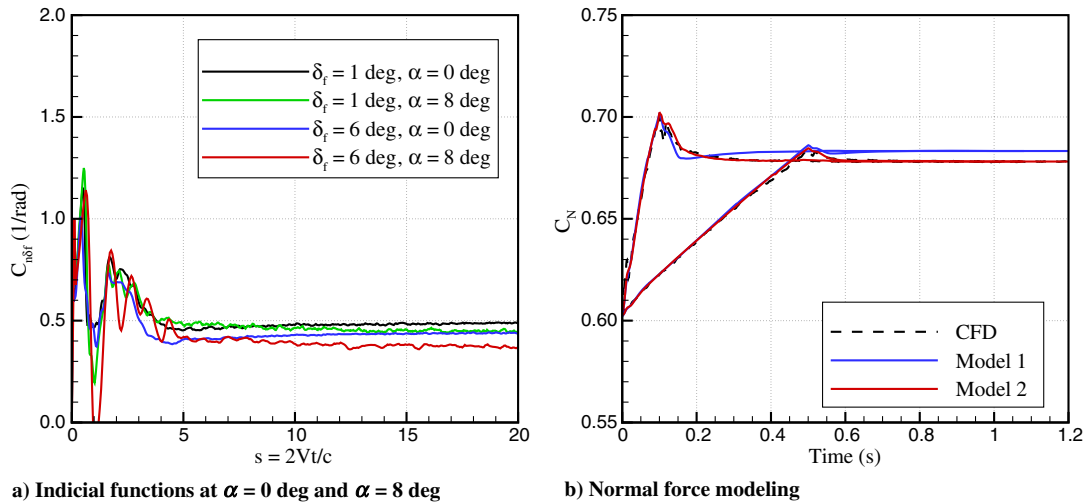


Fig. 24 Nonlinear normal force modeling of ramp-flap motions at 8 deg angle of attack.

response function calculations. The nonlinear effects are much more pronounced in the pitch moment than the normal force (as shown in Fig. 20); therefore, larger discrepancies are found between the CFD and the model predictions. The nonlinear models are also evaluated for different pitch-flap motions. The motions in Fig. 22 have an oscillation amplitude of 9 deg with reduced frequency values of 0.2 and 0.32. Figure 22 shows that the model agrees well with CFD predictions; hysteresis loops and initial loads are captured quite well. The nonlinear models are also tested for a large-amplitude pitch-flap motion, and the results are shown in Fig. 23. In this case, the motion is started from 15 deg flap deflection with an oscillation amplitude of 15 deg and reduced frequency of 0.098. Even for this motion, the model predictions are quite good.

2. Aerodynamic Modeling at α Equal to Eight Degrees

The next two ramp-flap motions at 8 deg angle of attack are tested. The motions are started from a clean configuration, and then the flap is deflected from 0 to 10 deg with rates of 20 and 100 deg/s and is held constant at 10 deg. Figure 24a compares the flap response functions at 0 and 8 deg angles of attack. The results show that responses change with angle of attack such that responses become smaller at 8 deg; this confirms that flap responses depend on the angle of attack as well as the flap angle. Figure 24b compares the CFD normal force data with two reduced-order models. The first model (Model 1 in Fig. 24b) is created from responses at 0 deg angle of attack, and the second model (Model 2 in Fig. 24b) is created from

responses at 8 deg angle of attack. The results show that the first model overestimates the CFD prediction, but the second model produces a good match. These results confirm that flap responses should be generated separately for each angle of attack in the input space. However, this makes aerodynamic modeling over a large region of the input space expensive. Therefore, a time-dependent surrogate model is proposed to approximate flap responses from a small response simulations or samples.

3. Aerodynamic Modeling in $\delta_f - \alpha$ Space

A nonlinear indicial response method, along with a time-dependent surrogate approach, is proposed for normal force modeling in the angle of attack/flap angle space. In this model, the indicial function in the input space of angle of attack/flap angle are interpolated from some available samples. An input space of α and δ_f is defined by assuming a range of [0, 8 deg] for α and [-10, 10 deg] for δ_f . A set of samples including 15 points is then defined on this space and is shown in Fig. 25. The samples are selected at different angles of attack, mainly at large flap angles. These samples include positive flap angles, assuming that the normal force is symmetric with flap angle. Next, the flap responses are calculated using time-accurate CFD for each sample condition. A new ROM is then created using Eq. (3) and used to predict the normal force acting on the aircraft due to arbitrary flap motion at any given angle of attack within the range of data used for the model creation. The surrogate model described in Sec. II aids in approximating the response dependence on the angle of attack and flap angle. The validity of the ROM is tested for several arbitrary motions at angles of attack not simulated in the sample design. Figure 26 compares the model predictions with time-accurate CFD simulations of these motions. This figure shows that the ROM predictions agree quite well with the CFD for all motions.

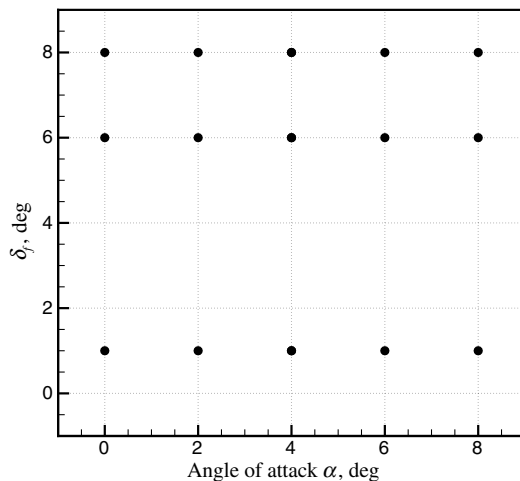


Fig. 25 Samples design for surrogate modeling of flap aerodynamics at different α .

V. Conclusions

This paper extends the previous work on unsteady aerodynamic modeling using indicial response methods by modeling aircraft control surfaces. The step-type response in control-surface deflections were directly calculated from unsteady RANS simulations and an overset grid technique. The results showed that indicial normal force responses due to a unit step change in flap and elevator have an initial jump as the grid starts to rotate, followed by a transient solution. As time progresses, the normal force asymptotically reached the steady-state value corresponding to 1 deg flap or elevator angle. Pitch moment responses also showed an initial negative peak and a transient solution until they reach the steady-state values. However, the final-time pitch moment response was positive for the flap and was negative for the elevator due to the location of the flap and elevator relative to the moment reference point. The aileron indicial functions had large

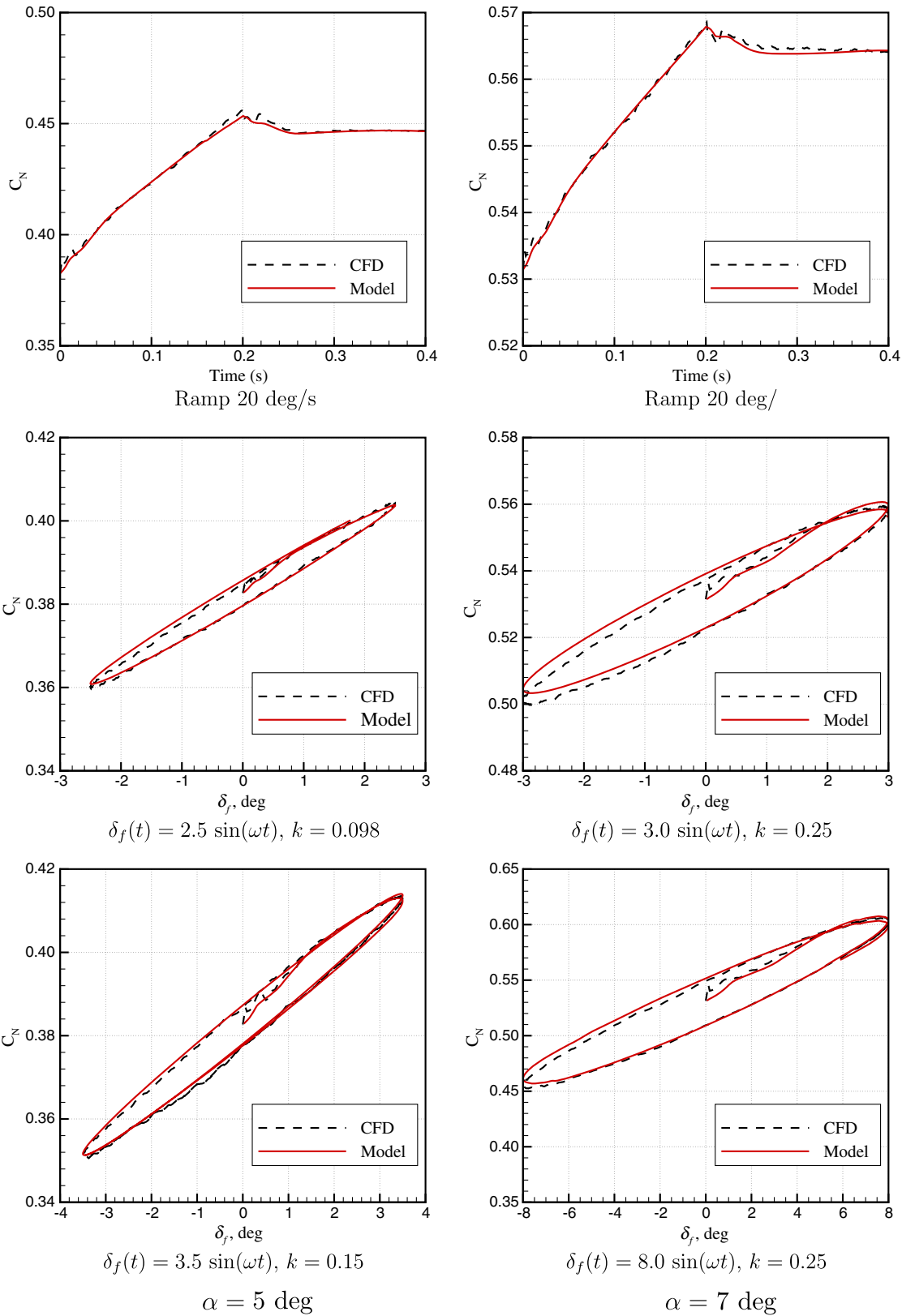


Fig. 26 Aerodynamic modeling in angle-of-attack and flap-angle input space.

oscillations initially and then reach the steady-state solutions at 1 deg aileron angle. The results showed that indicial values of side-force and yaw moment are much smaller than roll moment.

The linear models using these indicial functions produced accurate predictions for small-amplitude flap motions, but they overestimated large amplitude motions. The results showed that the nonlinear models gave better predictions compared with the linear model, but it

is more expensive because it used more response functions at different flap angles. Also, it was shown that response functions depend on both angle of attack and flap angle. This makes model creation more expensive because a large number of response functions need to be calculated for each combination of angle of attack and flap angle. A method to efficiently reduce the number of step function calculations was then used. This method uses

a time-dependent surrogate model to fit the relationship between flight conditions (angle of attack and flap angle) and step functions calculated for a limited number of samples. This method was used to approximate the normal force responses induced by arbitrary flap motions at a given angle of attack. Again, a good agreement between CFD and model output was found. Comparisons of CFD and steady-state solutions confirmed the previous experiments that unsteady effects significantly change the amplitude and phase lags of predicted airloads. Future work will extend the results to include aerodynamic modeling of very large flap angles and validation of aerodynamic models for a generic unmanned combat air vehicle with trailing-edge flaps with available experimental data.

Acknowledgments

Mehdi Ghoreyshi is supported by the U.S. Air Force Academy (USAFA) under contract FA70001320018; their financial support is gratefully acknowledged. Computational grids were generated by Adam Jirasek. Acknowledgments are expressed to the U.S. Department of Defense High Performance Computing Modernization Program, Engineering Research Development Center, and U.S. Air Force Research Labs for providing computer time. The authors appreciate the support provided by the High Performance Computing Research Center at USAFA. Special thanks are also due to David Findlay and Brad Green of Naval Air Systems Command for their helpful comments.

References

- Rennie, R. M., and Jumper, E. J., "Dynamic Leading-Edge Flap Scheduling," *13th Applied Aerodynamics Conference*, AIAA Paper 1995-1904, June–July 1995.
- Molina, J., and Zhang, X., "Aerodynamics of a Heaving Airfoil in Ground Effect," *AIAA Journal*, Vol. 49, No. 6, 2011, pp. 1168–1179. doi:10.2514/1.J050369
- Vieira, B. A., Kinzel, M. P., and Maughmer, M. D., "Unsteady Aerodynamics of Miniature Trailing-Edge Effectors Based on Indicial Methods," *49th AIAA Aerospace Sciences Meeting*, AIAA Paper 2011-1049, Jan. 2011.
- McDaniel, D. R., Sears, D. R., Tuckey, T. R., Tillman, B., and Morton, S. A., "Aerodynamic Control Surface Implementation in Kestrel v2.0," *49th AIAA Aerospace Sciences Meeting*, AIAA Paper 2011-1175, Jan. 2011.
- Schütte, A., Einarsson, G., Raichle, A., Schoning, B., Mönnich, W., and Forkert, T., "Numerical Simulation of Maneuvering Aircraft by Aerodynamic, Flight Mechanics, and Structural Mechanics Coupling," *Journal of Aircraft*, Vol. 46, No. 1, 2009, pp. 53–64. doi:10.2514/1.31182
- Ghoreyshi, M., Vallespin, D., DaRonch, A., Badcock, K. J., Vos, J., and Hitzel, S., "Simulation of Aircraft Manoeuvres based on Computational Fluid Dynamics," *AIAA Atmospheric Flight Mechanics Conference*, AIAA Paper 2010-8239, Aug. 2010.
- Stark, V. J. E., "Indicial Coefficients for a Cropped Delta Wing in Incompressible Flow," *Journal of Aircraft*, Vol. 23, No. 5, 1986, pp. 370–375. doi:10.2514/3.45317
- Lisandrin, P., Carpentieri, G., and van Tooren, M., "Investigation over CFD-Based Models for the Identification of Nonlinear Unsteady Aerodynamics Responses," *AIAA Journal*, Vol. 44, No. 9, 2006, pp. 2043–2050. doi:10.2514/1.18726
- Leishman, J. G., *Principles of Helicopter Aerodynamics*, Cambridge Univ. Press, New York, 2006, pp. 322–332.
- Wagner, H., "Über die Entstehung des Dynamischen Auftriebes von Tragflügeln," *Zeitschrift für Angewandte Mathematik und Mechanik*, Vol. 5, No. 1, 1925, pp. 17–35. doi:10.1002/zamm.19250050103
- Tobak, M., "On the Use of the Indicial Function Concept in the Analysis of Unsteady Motions of Wings and Wing–Tail Combinations," NACA Rept. 1188, 1954.
- Ghoreyshi, M., and Cummings, R. M., "Unsteady Aerodynamics Modeling for Aircraft Maneuvers: A New Approach Using Time-Dependent Surrogate Modeling," *30th AIAA Applied Aerodynamics Conference*, AIAA Paper 2012-3327, June 2012.
- Hariharan, N., and Leishman, J. G., "Unsteady Aerodynamics of a Flapped Airfoil in Subsonic Flow by Indicial Concepts," *Journal of Aircraft*, Vol. 33, No. 5, 1996, pp. 855–868. doi:10.2514/3.47028.
- Nakai, K., Shimoyama, K., Obayashi, S., Morino, H., and Yamaguchi, H., "Calculation of Unsteady Control Surface Aerodynamics Using Reduced-Order Models," *49th AIAA Aerospace Sciences Meeting*, AIAA Paper 2011-1048, Jan. 2011.
- Strang, W. Z., Tomaro, R. F., and Grismer, M. J., "The Defining Methods of Cobalt: A Parallel, Implicit, Unstructured Euler/Navier–Stokes Flow Solver," *37th Aerospace Sciences Meeting and Exhibit*, AIAA Paper 1999-0786, Jan. 1999.
- Gottlieb, J. J., and Groth, C. P. T., "Assessment of Riemann Solvers for Unsteady One-Dimensional Inviscid Flows of Perfect Gasses," *Journal of Fluids and Structure*, Vol. 78, No. 2, 1998, pp. 437–458. doi:10.1016/0021-9991(88)90059-9
- Tomaro, R. F., Strang, W. Z., and Sankar, L. N., "An Implicit Algorithm for Solving Time Dependent Flows on Unstructured Grids," *35th Aerospace Sciences Meeting and Exhibit*, AIAA Paper 1997-0333, Jan. 1997.
- Spalart, P. R., and Allmaras, S. R., "A One Equation Turbulence Model for Aerodynamic Flows," *30th Aerospace Sciences Meeting and Exhibit*, AIAA Paper 1992-0439, Jan. 1992.
- Wilcox, D. C., "Reassessment of the Scale Determining Equation for Advanced Turbulence Models," *AIAA Journal*, Vol. 26, No. 11, 1988, pp. 1299–1310. doi:10.2514/3.10041
- Menter, F., "Eddy Viscosity Transport Equations and Their Relation to the k - ϵ Model," *ASME Journal of Fluids Engineering*, Vol. 119, No. 4, 1997, pp. 876–884. doi:10.1115/1.2819511
- Stephens, C. H., Arena, A. S., and Gupta, K. K., "Application of the Transpiration Methods for Aeroservoelastic Prediction Using CFD," *39th AIAA/ASME/ASCE/AHS/ASC Structures, Structural Dynamics, and Materials Conference and Exhibit*, AIAA Paper 1998-2071, April 1998.
- Stephens, C. H., Arena, A. S., and Gupta, K. K., "CFD-Based Aeroservoelastic Prediction with Comparisons to Benchmark Experimental Data," *37th Aerospace Sciences Meeting and Exhibit*, AIAA Paper 1999-0766, Jan. 1999.
- Ghoreyshi, M., DaRonch, A., Vallespin, D., Badcock, K. J., Mengmeng, Z., Ooppelstrup, J., and Rizzi, A., "A Framework for Constrained Control Allocation Using CFD-Based Tabular Data," *49th AIAA Aerospace Sciences Meeting*, AIAA Paper 2011-0925, Jan. 2011.
- Raveh, D. E., "Maneuver Load Analysis of Over-Determined Trim Systems," *Journal of Aircraft*, Vol. 45, No. 1, 2008, pp. 119–129. doi:10.2514/1.29118
- Randall, T. C. S., and Allen, C. B., "Efficient Mesh Motion Using Radial Basis Functions with Data Reduction Algorithms," *Journal of Computational Physics*, Vol. 228, No. 17, 2009, pp. 6231–6249. doi:10.1016/j.jcp.2009.05.013
- Ghoreyshi, M., Badcock, K. J., Da Ronch, A., Marques, S., Swift, A., and Ames, N., "Framework for Establishing the Limits of Tabular Aerodynamic Models for Flight Dynamics Analysis," *Journal of Aircraft*, Vol. 48, No. 1, 2011, pp. 42–55. doi:10.2514/1.C001003
- Michler, A. K., "Aircraft Control Surface Deflection Using RBF-Based Mesh Deformation," *International Journal for Numerical Methods in Engineering*, Vol. 88, No. 10, 2011, pp. 986–1007. doi:10.1002/nme.3208
- Potsdam, M. A., and Guruswamy, G. P., "A Parallel Multiblock Mesh Movement Scheme for Complex Aeroelastic Applications," *39th Aerospace Sciences Meeting and Exhibit*, AIAA Paper 2001-0716, Jan. 2001.
- Batina, J. T., "Unsteady Euler Algorithm with Unstructured Dynamic Mesh for Complex Aircraft Aeroelastic Analysis," *30th Structures, Structural Dynamics and Materials Conference*, AIAA Paper 1989-1189, June 1989.
- Bartles, R. E., "An Elasticity-Based Mesh Scheme Applied to the Computation of Unsteady Three-Dimensional Spoiler and Aeroelastic Problems," *14th Computational Fluid Dynamics Conference*, AIAA Paper 1999-3301, June 1999.
- Farhat, C., Degand, B., Koobus, B., and Lesoinne, M., "An Improved Method of Spring Analogy for Dynamic Unstructured Fluid Meshes," *AIAA Structural Dynamics and Material Conference*, AIAA Paper 1998-2070, April 1998.
- Biswas, R., *Parallel Computational Fluid Dynamics: Recent Advances and Future Directions*, DEStech Publ., Lancaster, PA, 2010, pp. 535–538.
- Satofuka, N., *Computational Fluid Dynamics*, Springer-Verlag, Berlin, 2001, pp. 8–9.

- [34] Liggett, N., and Smith, M. J., "The Physics of Modeling Unsteady Flaps With Gaps," *Journal of Fluids and Structures*, Vol. 38, April 2013, pp. 255–272.
doi:10.1016/j.jfluidstructs.2012.12.010
- [35] Tuncer, I. H., Gulcat, U., Emerson, D. R., and Matsuno, K., *Parallel Computational Fluid Dynamics 2007*, Springer-Verlag, Berlin, 2009, pp. 211–213.
- [36] Ghoreyshi, M., Jirasek, A., and Cummings, R. M., "Computational Investigation into the Use of Response Functions for Aerodynamic Loads Modeling," *AIAA Journal*, Vol. 50, No. 6, 2012, pp. 1314–1327.
doi:10.2514/1.J051428
- [37] Ghoreyshi, M., Cummings, R. M., Da Ronch, A., and Badcock, K. J., "Transonic Aerodynamic Load Modeling of X-31 Aircraft Pitching Motions," *AIAA Journal*, Vol. 51, No. 10, 2013, pp. 2447–2464.
doi:10.2514/1.J052309
- [38] Ghoreyshi, M., Post, M. L., and Cummings, R. M., "CFD Calculation of Aerodynamic Indicial Functions for a Generic Fighter Configuration," *ITEA Journal of Test and Evaluation*, Vol. 33, No. 6, 2012, pp. 348–364.
- [39] Duffy, D. G., *Advanced Engineering Mathematics with MATLAB*, 2nd ed., CRC Press, Boca Raton, FL, 2003, pp. 748–750.
- [40] Tobak, M., and Schiff, L. B., "On the Formulation of the Aerodynamic Characteristics in Aircraft Dynamics," NASA TR-R-456, 1976.
- [41] Brandt, S., Stiles, R., Bertin, J. J., and Whitford, R., *Introduction to Aeronautics: A Design Perspective*, 2nd ed., AIAA Education Series, AIAA, Reston, VA, 2004, pp. 476–492.
- [42] Mueller, M., *Thunderbird Milestones*, MBI Publ., Osceola, WI, 1999, pp. 80–81.
- [43] Tyssel, L., "Hybrid Grid Generation for Complex 3D Geometries," *Proceedings of the 7th International Conference on Numerical Grid Generation in Computational Field Simulation*, Whistler, British Columbia, Canada, 2000, pp. 337–346.
- [44] Tyssel, L., "The TRITET Grid Generation System," *Proceedings of the 10th International Conference on Numerical Grid Generation in Computational Field Simulations*, Heraklion, Crete, Greece, Sept. 2000.
- [45] Ghoreyshi, M., and Cummings, R. M., "Challenges in the Aerodynamics Modeling of an Oscillating and Translating Airfoil at Large Incidence Angles," *Aerospace Science and Technology*, Vol. 28, No. 1, 2013, pp. 176–190.
doi:10.1016/j.ast.2012.10.013

W. Silva
Associate Editor